

THE COMPUTATION OF CONICAL DIFFRACTION COEFFICIENTS IN HIGH-FREQUENCY ACOUSTIC WAVE SCATTERING*

B.D. BONNER[†], I.G. GRAHAM[‡], AND V.P. SMYSHLYAEV[§]

Abstract. When a high-frequency acoustic or electromagnetic wave is scattered by a surface with a conical point, the component of the asymptotics of the scattered wave corresponding to diffraction by the conical point can be represented as an asymptotic expansion, valid as the wave number $k \rightarrow \infty$. The *diffraction coefficient* is the coefficient of the principal term in this expansion and is of fundamental interest in high-frequency scattering. It can be computed by solving a family of homogeneous boundary value problems for the Laplace-Beltrami-Helmholtz equation (parametrised by a complex wave number-like parameter ν), on a portion of the unit sphere bounded by a simple closed contour ℓ , and then integrating the resulting solutions with respect to ν . In this paper we give the numerical analysis of a method for carrying out this computation (in the case of acoustic waves) via the boundary integral method applied on ℓ , emphasising the practically important case when the conical scatterer has lateral edges. The theory depends on an analysis of the integral equation on ℓ , which shows its relation to the corresponding integral equation for the planar Helmholtz equation. This allows us to prove optimal convergence for piecewise polynomial collocation methods of arbitrary order. We also discuss efficient quadrature techniques for assembling the boundary element matrices. We illustrate the theory with computations on the classical canonical open problem of a trihedral cone.

Keywords: Acoustic wave scattering, high-frequency asymptotics, diffraction coefficients, conical points, lateral edges, boundary integral method, collocation, mesh grading, convergence.

Mathematics Subject Classification (MSC 2000): 65N38, 65R20, 35P25, 78A45

Running Head: Computation of Conical Diffraction Coefficients

1. Introduction. When an incident plane acoustic or electromagnetic wave is scattered by a bounded impenetrable (3D) obstacle, the asymptotic behaviour of the scattered wave when the frequency is large is described by the classical Geometric Theory of Diffraction (GTD) [27]. The asymptotics of the scattered field when the wave number $k \rightarrow \infty$ is known from the GTD to be composed of a number of components corresponding to “reflections” or “diffractions” by particular parts of the boundary. As well as the component corresponding to simple reflection of non-grazing incident waves at smooth parts of the obstacle, or a more complicated grazing incidence which leads to asymptotics in the shadow [26] and special boundary-layer asymptotics in the “penumbra” (see e.g. [7] and further references therein), the scattered wave’s asymptotics may also contain components arising from diffraction by non-smooth “singular” points of the scattering surface, such as edges or conical points. From the GTD [27] (and its further developments), the principal parts of those components are known to be described by the (diffracted component of the) far field of waves scattered by the *tangent cone* at the singular point(s). This is due to the so-called “principle of localisation” (which is the essence of the GTD). Many authors have considered the problem of describing the asymptotics of the diffracted wave for various “canonical” cones (see e.g [12, 15, 11, 6] and further references therein).

When the obstacle is a cone with a smooth lateral surface and ideal boundary conditions are applied, this problem has been studied in detail by many authors, see e.g. [12],[6] and further references therein, where explicit formulae for the principal asymptotics of the diffracted wave were derived. (By “ideal” we mean pure Dirichlet or Neumann boundary conditions in the acoustic case and perfectly conducting boundary conditions in the electromagnetic case. See [9, 2, 10] for some results on non-ideal boundary conditions.)

For example, consider the scalar (acoustic) case, with an incident plane wave $U^{inc}(\mathbf{x}) = \exp(-ik\boldsymbol{\omega}_0 \cdot \mathbf{x})$, with the point $\boldsymbol{\omega}_0 \in S^2$ (the unit sphere in \mathbb{R}^3), describing the direction of incidence. Then, both the scattered wave U^{sc} and the total wave $U := U^{inc} + U^{sc}$ satisfy the 3D Helmholtz equation, $(\Delta + k^2)U = 0$, in the domain of propagation, and U^{sc} satisfies an appropriate version of the radiation conditions. The theory in [32], [4] and [6] describes the behaviour of the diffracted component $U^{diff}(\mathbf{x})$ of $U^{sc}(\mathbf{x})$ at any point \mathbf{x} in the domain of propagation. Using spherical coordinates centred at the conical point: $\mathbf{x} = r\boldsymbol{\omega}$ with $\boldsymbol{\omega} \in S^2$ and $r > 0$ denoting the distance of \mathbf{x} from the conical point, it follows from the general recipes of the GTD that (with either Dirichlet or Neumann conditions imposed on the surface of the scatterer), U^{diff} has the asymptotic representation

$$(1.1) \quad U^{diff}(\mathbf{x}, k, \boldsymbol{\omega}_0) = 2\pi \frac{\exp(ikr)}{kr} f(\boldsymbol{\omega}, \boldsymbol{\omega}_0) + O((kr)^{-2}), \quad k \rightarrow \infty.$$

*This work was completed while the second author was visiting the programme on Computational Challenges in PDEs at the Newton Institute for Mathematical Sciences, Cambridge, UK.

[†]bradley_bonner@yahoo.co.uk

[‡]Mathematical Sciences, University of Bath, Bath BA2 7AY, U.K. (I.G.Graham@bath.ac.uk)

[§]Mathematical Sciences, University of Bath, Bath BA2 7AY, U.K. (vps@maths.bath.ac.uk)

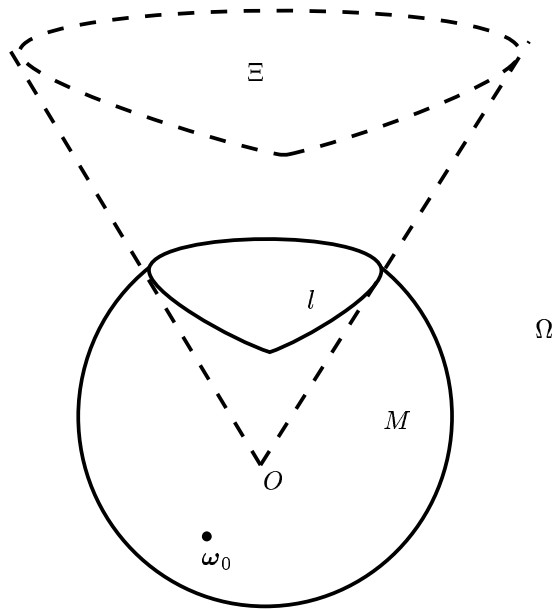


FIG. 1.1. *Geometry of obstacle*

Here the distribution $f(\boldsymbol{\omega}, \boldsymbol{\omega}_0)$, which is infinitely smooth everywhere except at the so-called “*singular directions*” (where it is typically infinite), is the important “*diffraction coefficient*” (also known as the kernel of the “*scattering matrix*”), and describes the intensity of the diffracted wave in the particular direction $\boldsymbol{\omega}$. (See, e.g. [6, 13] and further references therein for precise descriptions of the distributional spaces.)

This paper is about the numerical analysis and implementation of methods for computing $f(\boldsymbol{\omega}, \boldsymbol{\omega}_0)$. Following [4] and [6], to obtain a formula for f , we take O to be the vertex of the conical obstacle, Ξ , (which is indicated by dotted lines in Fig 1.1) and let M denote the portion of the unit sphere S^2 which is exterior to Ξ . M is a sub-manifold of S^2 with boundary which we denote by ℓ (see again Fig 1.1). Let Δ^* denote the Laplace-Beltrami operator on S^2 and introduce the “*spherical*” Green’s function $g(\boldsymbol{\omega}, \boldsymbol{\omega}_0, \nu)$ on M (also known as a “*spectral function*”), satisfying:

$$(1.2) \quad (\Delta^* + \nu^2 - 1/4)g(\boldsymbol{\omega}, \boldsymbol{\omega}_0, \nu) = \delta(\boldsymbol{\omega} - \boldsymbol{\omega}_0), \quad \boldsymbol{\omega}, \boldsymbol{\omega}_0 \in M \quad \text{and } \nu \in \mathbb{C},$$

where δ denotes the Dirac delta function and the differentiation on the left-hand side is with respect to $\boldsymbol{\omega}$. As a function of $\boldsymbol{\omega}$, g is also required to satisfy a Dirichlet or Neumann boundary condition on ℓ (whichever is given in the original scattering problem). Once g is known, the diffraction coefficient in (1.1) is then given by the formula (see: [32, 6])

$$(1.3) \quad f(\boldsymbol{\omega}, \boldsymbol{\omega}_0) = \lim_{s \rightarrow 0^+} \frac{i}{\pi} \int_{\gamma} \exp(-i\nu\pi - s\nu)g(\boldsymbol{\omega}, \boldsymbol{\omega}_0, \nu)\nu d\nu.$$

The integrals in (1.3) are known to converge uniformly as $s \rightarrow 0^+$ away from the singular directions, cf. [8]. The infinite integration contour γ in (1.3) has to be chosen in the complex plane, so that the (positive) numbers $\sqrt{\lambda_j}$ (where λ_j ranges over all eigenvalues of the self-adjoint operator $-\Delta^* + 1/4$ on M , subject to the appropriate boundary condition on ℓ) lie on its right and also so that when $\text{Re}(\nu) \rightarrow \infty$, along γ , $\text{Im}(\nu) \rightarrow \pm a$ for some constant $a > 0$ ([6]). The function $g(\boldsymbol{\omega}, \boldsymbol{\omega}_0, \nu)$ is known from spectral theory to be analytic in ν , except for poles at $\nu = \sqrt{\lambda_j}$, provided $\boldsymbol{\omega} \neq \boldsymbol{\omega}_0$ – see Figure 1.2.

Thus the computational procedure for realising the asymptotic formula (1.1) requires: (i) the computation of the Green’s function $g(\boldsymbol{\omega}, \boldsymbol{\omega}_0, \nu)$ for all required incidence directions $\boldsymbol{\omega}_0$ and observation directions $\boldsymbol{\omega} \in M$ and (ii) the computation of the integral in (1.3) for sufficiently small positive s , by quadrature. Note that (ii) in turn implies that $g(\boldsymbol{\omega}, \boldsymbol{\omega}_0, \nu)$ must be evaluated for sufficiently many $\nu \in \gamma$ to ensure an accurate answer.

The Green’s function g in (1.3) can be replaced ([32, 4]) by its regular part $g^r := g - g_0$, where g_0 is the (known) fundamental solution for the operator $(\Delta^* + \nu^2 - 1/4)$ on all of S^2 (see §2). Moreover, for certain configurations of $\boldsymbol{\omega}, \boldsymbol{\omega}_0$ (which, say, in the case of a smooth, fully illuminated and convex cone corresponds to the direction of observation $\boldsymbol{\omega}$ with no reflected wave [32, 4, 24] – see (2.1) for a precise statement), the

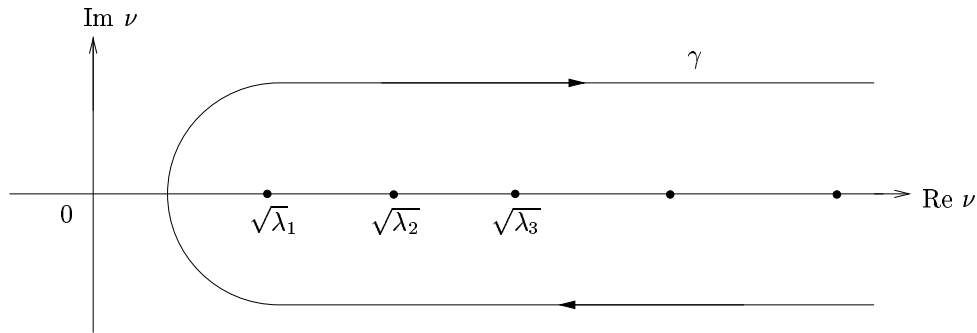


FIG. 1.2. *Contour of integration*

right-hand side of (1.3) can be transformed by deforming the contour of integration γ onto the imaginary axis and then interchanging the limit with the integral. These modifications yield the simpler formula:

$$(1.4) \quad f(\boldsymbol{\omega}, \boldsymbol{\omega}_0) = -\frac{i}{\pi} \int_{-\infty}^{\infty} \exp(\tau\pi) g^r(\boldsymbol{\omega}, \boldsymbol{\omega}_0, i\tau) \tau d\tau,$$

with the integral convergent absolutely. In fact it can be shown (see [13, §6.4] and the references therein) that

$$(1.5) \quad \exp(\tau\pi) g^r(\boldsymbol{\omega}, \boldsymbol{\omega}_0, i\tau) \sim \begin{cases} \exp(\alpha_1 \tau), & \tau \rightarrow -\infty, \\ \exp(-\alpha_2 \tau), & \tau \rightarrow \infty, \end{cases}$$

where α_1, α_2 are positive numbers depending on the location of $\boldsymbol{\omega}$ and $\boldsymbol{\omega}_0$, provided $\boldsymbol{\omega}$ and $\boldsymbol{\omega}_0$ satisfy the technical condition (2.1) below.

The configurations of $\boldsymbol{\omega}$ and $\boldsymbol{\omega}_0$ for which the formulation (1.4) is possible are described by a geometrical condition (see [6, §2.3]). All our computations in this paper are for cases in which (1.4) is valid. In other cases one must compute the limit (1.3) as it stands, leading to a more complicated approximation problem directly employing (1.3) with sufficiently small s [6].

In [4] and [6] a numerical method was proposed for the computation of (1.4) and (1.3). The boundary integral method was used to compute g^r . (g^r satisfies the homogeneous PDE $(\Delta^* + \nu^2 - 1/4)g^r(\boldsymbol{\omega}, \boldsymbol{\omega}_0, \nu) = 0$, on the manifold M , subject to an inhomogeneous boundary condition on its boundary ℓ .) This was implemented in [4] and [6] in the case when Ξ is a smooth cone (i.e. ℓ is a smooth contour) using, in effect, a simple trapezoidal-Nyström type integral equation solver combined with the trapezoidal rule for computing (1.3) or (1.4). The approach of [32],[4] and [6] was also extended to the electromagnetic case [33], which was implemented numerically in [5].

The papers [4] and [6] contained no convergence analysis of the method and moreover, they dealt only with the case of a smooth cone Ξ . The case of a cone with lateral edges is of fundamental importance in both the high-frequency theory of diffraction (where it is one of the unsolved canonical problems [27]) and in practice, where high frequency scattering by antennae or corners of buildings is a key problem in microwave engineering. In such cases ℓ contains corners.

Although the integral equation method reduces the computation of $g(\boldsymbol{\omega}, \boldsymbol{\omega}_0, \nu)$ to a computation on the (1D) contour ℓ on the surface of the unit sphere S^2 , this equation has to be solved many times for different values of ν (and also more times if different $\boldsymbol{\omega}$ and $\boldsymbol{\omega}_0$ are to be considered). Moreover, as we shall see, the evaluation of the kernel in the integral equation arising from the spherical PDE (1.2) is much more costly than for typical boundary integral equations in planar scattering theory. Thus there is strong practical demand for the development of an efficient algorithm, in particular one which solves the integral equation with the highest accuracy and the minimal number of kernel evaluations. Thus the purposes of this paper are

- (i) To propose an efficient method for computing diffraction coefficients which is robust even when the cone Ξ has lateral edges and analyse its convergence;
- (ii) To minimise the number of kernel evaluations required in the implementation;
- (iii) To demonstrate its use in the computation of diffraction coefficients in several sample cases.

The plan of the paper is as follows. In §2 we describe briefly the boundary integral method for computing g^r . This leads to non-standard integral equations posed on the spherical contour ℓ , which possibly contains corners. In §3 we obtain the important properties of the integral operators which arise, including the case when the cone Ξ has lateral edges. In §4 we describe a flexible numerical method based on collocation with piecewise

polynomials and we prove its convergence as a means of approximating $g^r(\boldsymbol{\omega}, \boldsymbol{\omega}_0, \nu)$. Finally in §5 we provide computations of diffraction coefficients for several sample problems. We also give in §5 outline descriptions of various technical issues such as the computation of the contour integral in (1.3) and the evaluation of the kernel which appears in the integral operator. In particular, we note that because of the exponential decay (1.5), the domain of integration in (1.4) can be replaced by $[-N_1, N_2]$ with $N_i = O(r \log(n))$ at the cost of an error of $O(1/n^r)$. Therefore very large values of N_i (equivalently very large values of $|\tau|$) are not required in our computations.

Although this paper considers only diffraction coefficients for acoustic scattering, the related and more difficult electromagnetic case is described in [13] and the references therein.

2. Formulae for the Conical Diffraction Coefficients. Throughout the paper we shall assume that the cone Ξ has a finite number of smooth (analytic) faces, joined at lateral edges, and that the angle between pairs of adjacent faces lies in $(0, 2\pi)$ (i.e. cuspid edges are excluded). As in [13], we also assume that M and $S^2 \setminus \overline{M}$ are simply connected subsets of S^2 and that the contour ℓ is a simple closed curve, consisting of a finite number of analytic arcs, also joined at non-cuspid corners. (For much of what we are going to do below, weaker smoothness assumptions away from edges would suffice, but we suppress this extra generality in the interests of readability.)

For $\boldsymbol{\omega}, \boldsymbol{\omega}' \in S^2$ we define $\theta(\boldsymbol{\omega}, \boldsymbol{\omega}')$ to be the geodesic distance between two points $\boldsymbol{\omega}$ and $\boldsymbol{\omega}'$ on the sphere S^2 (i.e. $\cos \theta(\boldsymbol{\omega}, \boldsymbol{\omega}') = \boldsymbol{\omega} \cdot \boldsymbol{\omega}'$, $0 \leq \theta(\boldsymbol{\omega}, \boldsymbol{\omega}') \leq \pi$). The configurations of $\boldsymbol{\omega}$ and $\boldsymbol{\omega}_0$ which ensures that (1.3) can be rewritten as (1.4) can now be described (for a convex fully illuminated cone) by the following condition (see also [32]):

$$(2.1) \quad \theta_1(\boldsymbol{\omega}, \boldsymbol{\omega}_0) := \min_{\boldsymbol{\omega}' \in \ell} \{\theta(\boldsymbol{\omega}, \boldsymbol{\omega}') + \theta(\boldsymbol{\omega}', \boldsymbol{\omega}_0)\} > \pi.$$

When $\theta_1(\boldsymbol{\omega}, \boldsymbol{\omega}_0) \leq \pi$ the formula (1.3) may either be undefined on the so-called “singular directions” or may have to be interpreted in an appropriate distributional sense - for more details see [6, 24, 8]. We will not discuss this here but the reader may refer to [6] and [13] for more detail, including the case when the cone is not fully illuminated.

As mentioned in §1, the regular part g^r of the Green’s function g in (1.2) is defined by

$$(2.2) \quad g^r(\boldsymbol{\omega}, \boldsymbol{\omega}_0, \nu) = g(\boldsymbol{\omega}, \boldsymbol{\omega}_0, \nu) - g_0(\boldsymbol{\omega}, \boldsymbol{\omega}_0, \nu)$$

where g_0 is given by:

$$(2.3) \quad g_0(\boldsymbol{\omega}, \boldsymbol{\omega}', \nu) = -\frac{1}{4 \cos(\pi\nu)} P_{\nu - \frac{1}{2}}(-\cos \theta(\boldsymbol{\omega}, \boldsymbol{\omega}')),$$

with P_k denoting the Legendre special function of the first kind of index k (see e.g. [1, page 332]). It is well-known (see e.g. [32], [4], [6]) that g_0 satisfies:

$$(2.4) \quad (\Delta^* + \nu^2 - 1/4)g_0(\boldsymbol{\omega}, \boldsymbol{\omega}', \nu) = \delta(\boldsymbol{\omega} - \boldsymbol{\omega}'), \quad \boldsymbol{\omega}, \boldsymbol{\omega}' \in S^2,$$

(where the differentiation is with respect to $\boldsymbol{\omega}$), i.e. it is the fundamental solution for the operator $\Delta^* + \nu^2 - 1/4$ on all of the sphere S^2 . Comparing (2.4) and (1.2), we see that for each $\boldsymbol{\omega}_0 \in M$ and $\nu \in \mathbb{C}$, the function g^r , as a function of $\boldsymbol{\omega}$, satisfies the homogeneous PDE, ([4, 6])

$$(2.5) \quad (\Delta^* + \nu^2 - 1/4)g^r(\boldsymbol{\omega}, \boldsymbol{\omega}_0, \nu) = 0, \quad \boldsymbol{\omega} \in M,$$

subject to the boundary condition on ℓ

$$(2.6) \quad \left. \begin{array}{ll} \text{either} & g^r(\boldsymbol{\omega}, \boldsymbol{\omega}_0, \nu) = -g_0(\boldsymbol{\omega}, \boldsymbol{\omega}_0, \nu), & \text{the Dirichlet case} \\ \text{or} & (\partial g^r / \partial \mathbf{m})(\boldsymbol{\omega}, \boldsymbol{\omega}_0, \nu) = -(\partial g_0 / \partial \mathbf{m})(\boldsymbol{\omega}, \boldsymbol{\omega}_0, \nu), & \text{the Neumann case} \end{array} \right\} \text{ for all } \boldsymbol{\omega} \in \ell.$$

The boundary condition to be imposed on g^r is inherited from the boundary condition imposed on the original scattering problem. In (2.6) and throughout the paper, we make use of the following notational convention:

NOTATION 2.1. *With each $\boldsymbol{\omega} \in \ell$, not a corner point, we associate a unit normal $\mathbf{m} = \mathbf{m}(\boldsymbol{\omega})$ to ℓ at $\boldsymbol{\omega}$ which lies in the plane tangent to the unit sphere S^2 at $\boldsymbol{\omega}$ and is oriented outward from M . We also associate with $\boldsymbol{\omega}$ the unit tangent to ℓ at $\boldsymbol{\omega}$ denoted by $\mathbf{t} = \mathbf{t}(\boldsymbol{\omega})$, oriented so that $\mathbf{t}(\boldsymbol{\omega})$, $\mathbf{m}(\boldsymbol{\omega})$, $\boldsymbol{\omega}$ form an orthogonal right-handed triple (see Fig 3.1). (We usually suppress the dependence on $\boldsymbol{\omega}$ from the notation for simplicity.)*

Then $\partial/\partial\mathbf{m}$ denotes the (outward) normal derivative with respect to $\omega \in \ell$. For any other point ω' in ℓ , we analogously define the unit normal and tangent vectors \mathbf{m}' and \mathbf{t}' and normal derivative $\partial/\partial\mathbf{m}'$.)

The problem (2.5),(2.6) can now be solved by an integral equation method on ℓ . Here we follow the classical indirect approach, e.g. [3], adapted to the present problem in [4] and [6], although we note that a direct approach based on Green's formula would also be possible.

In the Dirichlet case, we seek the solution in the form of a double layer potential

$$(2.7) \quad g^r(\omega, \omega_0, \nu) = \int_{\ell} \frac{\partial g_0}{\partial \mathbf{m}'}(\omega, \omega', \nu) u(\omega', \nu) d\omega', \quad \omega \in M .$$

Taking limits as ω tends to the contour ℓ in (2.7) and using the jump conditions of the double layer potential and the Dirichlet boundary condition from (2.6), we obtain the second-kind integral equation:

$$(2.8) \quad \frac{1}{2}u(\omega, \nu) + \int_{\ell} \frac{\partial g_0}{\partial \mathbf{m}'}(\omega, \omega', \nu) u(\omega', \nu) d\omega' = -g_0(\omega, \omega_0, \nu),$$

for all smooth points $\omega \in \ell$. This equation is given in [4]. A rigorous justification for potential theory on manifolds with smooth boundaries is given in a very general context in [18]. For corner points the factor $1/2$ has to be replaced by a factor related to the corner angle, c.f. [14]. However, since we will estimate errors for our boundary integral equations in L^2 type spaces, these points are unimportant. Notice that, since $\omega \in \ell$ and $\omega_0 \in M$, the right-hand side (2.8) is never singular.

Analogously, the Neumann problem is solved with the single layer potential:

$$(2.9) \quad g^r(\omega, \omega_0, \nu) = \int_{\ell} g_0(\omega, \omega', \nu) u(\omega', \nu) d\omega', \quad \omega \in M .$$

Taking the normal derivative and fitting the boundary condition leads to:

$$(2.10) \quad -\frac{1}{2}u(\omega, \nu) + \int_{\ell} \frac{\partial g_0}{\partial \mathbf{m}}(\omega, \omega', \nu) u(\omega', \nu) d\omega' = -\frac{\partial g_0}{\partial \mathbf{m}}(\omega, \omega_0, \nu) .$$

We can write (2.8),(2.10) (almost everywhere) in operator form as

$$(2.11) \quad (I + \mathcal{L}_B)u = b_B , \quad \text{with } (\mathcal{L}_B u)(\omega) = \int_{\ell} L_B(\omega, \omega') u(\omega') d\omega' , \quad B = D, N,$$

with solution $u(\omega, \nu)$ abbreviated by $u(\omega)$. In the Dirichlet case the data is

$$(2.12) \quad b_D(\omega) := -2g_0(\omega, \omega_0, \nu) , \quad L_D(\omega, \omega') := 2 \frac{\partial g_0}{\partial \mathbf{m}'}(\omega, \omega', \nu) ,$$

and in the Neumann case,

$$(2.13) \quad b_N(\omega) := 2 \frac{\partial g_0}{\partial \mathbf{m}}(\omega, \omega_0, \nu) , \quad L_N(\omega, \omega') := -2 \frac{\partial g_0}{\partial \mathbf{m}}(\omega, \omega', \nu) .$$

Although the operators in (2.11), with the kernels from (2.12) or (2.13) are not classical, we will show that their properties are analogous to those of the standard layer potentials for the Helmholtz equation on the boundary of a planar domain.

3. Integral Operators.

3.1. Preliminary Results. The aim of this subsection is to identify the principal parts of the kernels L_D and L_N . This is done in Theorem 3.3. To prove this we need two technical lemmas.

LEMMA 3.1. *Using Notation 2.1, we have*

$$(3.1) \quad L_D(\omega, \omega') = \frac{1}{2 \cos(\pi\nu)} P'_{\nu-\frac{1}{2}}(-\cos \theta(\omega, \omega')) \mathbf{t}' \cdot (\omega \wedge \omega') ,$$

$$(3.2) \quad L_N(\omega, \omega') = -\frac{1}{2 \cos(\pi\nu)} P'_{\nu-\frac{1}{2}}(-\cos \theta(\omega, \omega')) \mathbf{t} \cdot (\omega' \wedge \omega) .$$

Proof. By employing spherical polar coordinates $\boldsymbol{\omega}' = (\sin \theta' \cos \phi', \sin \theta' \sin \phi', \cos \theta')^T$, for any $v : S^2 \rightarrow \mathbb{R}$, we have the representation

$$\frac{\partial v}{\partial \mathbf{m}'}(\boldsymbol{\omega}') = \nabla_{\boldsymbol{\omega}'} \{v \circ \boldsymbol{\omega}'\} \cdot \mathbf{m}' ,$$

where $\nabla_{\boldsymbol{\omega}'}$ is the spherical gradient:

$$\nabla_{\boldsymbol{\omega}'} = \frac{1}{\sin \theta'} \mathbf{e}_{\phi'} \frac{\partial}{\partial \phi'} + \mathbf{e}_{\theta'} \frac{\partial}{\partial \theta'} ,$$

with

$$\mathbf{e}_{\phi'} = (-\sin \phi', \cos \phi', 0)^T \quad \text{and} \quad \mathbf{e}_{\theta'} = (\cos \theta' \cos \phi', \cos \theta' \sin \phi', -\sin \theta')^T .$$

Since $\cos \theta(\boldsymbol{\omega}, \boldsymbol{\omega}') = \boldsymbol{\omega} \cdot \boldsymbol{\omega}'$, we have

$$(3.3) \quad \frac{\partial}{\partial \mathbf{m}'} P_{\nu-\frac{1}{2}}(-\cos \theta(\boldsymbol{\omega}, \boldsymbol{\omega}')) = -P'_{\nu-\frac{1}{2}}(-\cos \theta(\boldsymbol{\omega}, \boldsymbol{\omega}')) \nabla_{\boldsymbol{\omega}'} \{\boldsymbol{\omega} \cdot \boldsymbol{\omega}'\} \cdot \mathbf{m}' .$$

Now an easy calculation shows that

$$\nabla_{\boldsymbol{\omega}'} \{\boldsymbol{\omega} \cdot \boldsymbol{\omega}'\} \cdot \mathbf{m}' = \{(\boldsymbol{\omega} \cdot \mathbf{e}_{\phi'}) \mathbf{e}_{\phi'} + (\boldsymbol{\omega} \cdot \mathbf{e}_{\theta'}) \mathbf{e}_{\theta'}\} \cdot \mathbf{m}' = \boldsymbol{\omega} \cdot \mathbf{m}' .$$

Thus from (3.3), (2.3) and (2.12), we have

$$(3.4) \quad L_D(\boldsymbol{\omega}, \boldsymbol{\omega}') = \frac{1}{2 \cos(\pi\nu)} P'_{\nu-\frac{1}{2}}(-\cos \theta(\boldsymbol{\omega}, \boldsymbol{\omega}')) \boldsymbol{\omega} \cdot \mathbf{m}' .$$

Since \mathbf{t}' , \mathbf{m}' and $\boldsymbol{\omega}'$ form a right-handed triple, we have $\mathbf{m}' = \boldsymbol{\omega}' \wedge \mathbf{t}'$, and so

$$L_D(\boldsymbol{\omega}, \boldsymbol{\omega}') = \frac{1}{2 \cos(\pi\nu)} P'_{\nu-\frac{1}{2}}(-\cos \theta(\boldsymbol{\omega}, \boldsymbol{\omega}')) \boldsymbol{\omega} \cdot (\boldsymbol{\omega}' \wedge \mathbf{t}') ,$$

which is equivalent to (3.1) by cyclic permutation. Since $L_N(\boldsymbol{\omega}, \boldsymbol{\omega}') = -L_D(\boldsymbol{\omega}', \boldsymbol{\omega})$, (3.2) follows easily. \square

The next lemma identifies the asymptotic behaviour of $P'_{\nu+\frac{1}{2}}(x)$ for x close to -1 . In Theorem 3.3, we will combine this with (3.1), (3.2) to identify the behaviour of L_D and L_N near $\boldsymbol{\omega} = \boldsymbol{\omega}'$.

LEMMA 3.2. *For all $k \in \mathbb{C}$, $P_k(x)$ is an analytic function of $x \in (-1, 3)$. Moreover, for $x \in (-3, 1)$,*

$$P_k(x) = a_k(x) \log \left(\frac{1+x}{2} \right) + b_k(x) ,$$

where $a_k(x)$ and $b_k(x)$ are both analytic on $(-3, 1)$, with

$$a_k(-1) = \frac{\sin(\pi k)}{\pi} \quad \text{and} \quad b_k(-1) = \frac{\sin(\pi k)}{\pi} \{ \psi(k) + \psi(-k-1) + 2\gamma \} ,$$

where $\psi(k) = -\gamma - \sum_{r=1}^{\infty} (1/(k+r) - 1/r)$ and γ is the Euler constant ([1, p.255]).

Proof. From [1, equation 8.1.2] we get the following representation of P_k

$$(3.5) \quad P_k(x) = F(-k, k+1; 1; \frac{1-x}{2})$$

where F is the hypergeometric function. It follows from [1, page 556] that $F(-k, k+1; 1; z)$ is a convergent power series for $-1 \leq z < 1$. Therefore, by (3.5), $P_k(x)$ is analytic for $x \in (-1, 3)$ and in particular for $x \in (-1, 1)$. This proves the first statement in the theorem.

Furthermore from [23, Chapter V. equation 53] we have that

$$P_k(x) = a_k(x) \log \left(\frac{1+x}{2} \right) + b_k(x) ,$$

where

$$(3.6) \quad a_k(x) = \frac{\sin(\pi k)}{\pi} F(-k, k+1; 1; (1+x)/2)$$

and

$$(3.7) \quad b_k(x) = \frac{\sin(\pi k)}{\pi} \left\{ [\psi(k) + \psi(-k-1) + 2\gamma] F(-k, k+1; 1; (1+x)/2) + \sum_{r=1}^{\infty} B(k, r) \phi(k, r) \left(\frac{1+x}{2} \right)^r \right\}.$$

Here

$$B(k, r) = \frac{(-k) \dots (-k+r-1)(k+1) \dots (k+r)}{(r!)^2}$$

and

$$\phi(k, r) = \sum_{j=1}^r \left\{ \frac{2k(k+1) + j}{(j^2 - k^2 - k - j)j} \right\}.$$

As remarked above, $F(-k, k+1; 1; (1+x)/2)$ is a convergent power series for $-1 \leq (1+x)/2 < 1$, so $a_k(x)$ is analytic for $x \in (-3, 1)$. Moreover $a_k(-1) = \sin(\pi k)/\pi$ follows from [1, page 556].

Turning to b_k , it is clear that the first term on the right-hand side of (3.7) is also analytic for $x \in (-3, 1)$ and that the assertions about b_k will then follow provided the domain of convergence of the power series

$$(3.8) \quad \sum_{r=1}^{\infty} B(k, r) \phi(k, r) \left(\frac{1+x}{2} \right)^r$$

can be shown to be $(-3, 1)$. To obtain this result, note that $\lim_{r \rightarrow \infty} \phi(k, r)$ is clearly finite. If $\lim_{r \rightarrow \infty} \phi(k, r) \neq 0$ then it follows that $|\phi(k, r+1)/\phi(k, r)| \rightarrow 1$ as $r \rightarrow \infty$. Then

$$(3.9) \quad \lim_{r \rightarrow \infty} \frac{|B(k, r+1) \phi(k, r+1) ((1+x)/2)^{r+1}|}{|B(k, r) \phi(k, r) ((1+x)/2)^r|} = \left| \frac{1+x}{2} \right| \lim_{r \rightarrow \infty} \left| \frac{(-k+r)(k+r+1) \phi(k, r+1)}{(r+1)^2 \phi(k, r)} \right| = \left| \frac{1+x}{2} \right|,$$

and (3.8) is convergent for $x \in (-3, 1)$ by the ratio test. However if $\lim_{r \rightarrow \infty} \phi(k, r) = 0$ then, for large enough r , $|\phi(k, r)| < 1$. Since (3.9) also shows that the power series $\sum_{r=1}^{\infty} B(k, r) ((1+x)/2)^r$ converges for $x \in (-3, 1)$, the comparison test then ensures that (3.8) also converges for $x \in (-3, 1)$. \square

We now combine Lemmas 3.1 and 3.2 to obtain:

THEOREM 3.3. *Recall Notation 2.1.*

(i) For $\omega, \omega' \in \ell$,

$$(3.10) \quad L_D(\omega, \omega') = -\frac{\mathbf{t}' \cdot (\omega \wedge \omega')}{\pi |\omega - \omega'|^2} + F_D(\omega, \omega'),$$

$$(3.11) \quad L_N(\omega, \omega') = \frac{\mathbf{t} \cdot (\omega' \wedge \omega)}{\pi |\omega - \omega'|^2} + F_N(\omega, \omega'),$$

where F_D and F_N are bounded functions on $\ell \times \ell$.

(ii) When ω is not a corner point of ℓ ,

$$(3.12) \quad \frac{\mathbf{t}' \cdot (\omega \wedge \omega')}{\pi |\omega - \omega'|^2} \quad \text{and} \quad \frac{\mathbf{t} \cdot (\omega' \wedge \omega)}{\pi |\omega - \omega'|^2}$$

are both \mathcal{C}^∞ functions of ω' in a neighbourhood of ω and, for $B = D$ or N ,

$$(3.13) \quad F_B(\omega, \omega') = O(|\omega - \omega'|^2 \log |\omega - \omega'|), \quad \text{as } \omega' \rightarrow \omega.$$

Proof. We give the proof for L_D ; the argument for L_N is analogous.

(i) From Lemma 3.2 with $k = \nu - 1/2$, we have, for $x \in (-1, 1)$,

$$(3.14) \quad P'_{\nu-\frac{1}{2}}(x) = \frac{-\cos(\pi\nu)}{\pi} \left\{ \frac{1}{x+1} \right\} + r(x)$$

where

$$(3.15) \quad r(x) = \left[\frac{a_{\nu-\frac{1}{2}}(x) - a_{\nu-\frac{1}{2}}(-1)}{x - (-1)} + a'_{\nu-\frac{1}{2}}(x) \log \left(\frac{x+1}{2} \right) + b'_{\nu-\frac{1}{2}}(x) \right].$$

Also note that, since $\omega, \omega' \in S^2$, we have

$$(3.16) \quad -\cos \theta(\omega, \omega') + 1 = -\omega \cdot \omega' + 1 = \frac{1}{2} |\omega - \omega'|^2.$$

Hence

$$(3.17) \quad P'_{\nu-\frac{1}{2}}(-\cos \theta(\omega, \omega')) = -\frac{2 \cos(\pi\nu)}{\pi |\omega - \omega'|^2} + r(-1 + |\omega - \omega'|^2/2).$$

Therefore combining (3.1) with (3.15) and (3.17), we obtain the formula (3.10) where

$$(3.18) \quad F_D(\omega, \omega') = \frac{1}{2 \cos(\pi\nu)} r(-1 + |\omega - \omega'|^2/2) \mathbf{t}' \cdot (\omega \wedge \omega').$$

To complete the proof of (i) we now show that F_D is bounded on $\ell \times \ell$. To do this, choose a fixed δ satisfying $0 < \delta < \pi/2$ and first consider ω, ω' in the range

$$(3.19) \quad 0 \leq \theta(\omega, \omega') \leq \pi - \delta.$$

Then there exists $\epsilon > 0$ such that $-1 \leq -\cos \theta(\omega, \omega') \leq 1 - \epsilon$ and hence it follows from (3.16) that

$$(3.20) \quad -1 \leq -1 + |\omega - \omega'|^2/2 \leq 1 - \epsilon.$$

Substituting (3.15) into (3.18) we obtain

$$(3.21) \quad 2 \cos(\pi\nu) F_D(\omega, \omega') = \mathbf{t}' \cdot (\omega \wedge \omega') \left\{ \frac{a_{\nu-\frac{1}{2}}(-1 + |\omega - \omega'|^2/2) - a_{\nu-\frac{1}{2}}(-1)}{|\omega - \omega'|^2/2} + b'_{\nu-\frac{1}{2}}(-1 + |\omega - \omega'|^2/2) \right\}$$

$$(3.22) \quad + a'_{\nu-\frac{1}{2}}(-1 + |\omega - \omega'|^2/2) \left\{ \mathbf{t}' \cdot (\omega \wedge \omega') \log(|\omega - \omega'|^2/4) \right\}.$$

Recall from Lemma 3.2 that $a_{\nu-\frac{1}{2}}$ and $b'_{\nu-\frac{1}{2}}$ are both analytic on $(-3, 1)$. Since $|\omega - \omega'|^2$ is a smooth function of ω, ω' , it follows that the terms inside the braces in (3.21) are smooth functions of $\omega, \omega' \in \ell$. Moreover

$$(3.23) \quad \begin{aligned} |\mathbf{t}' \cdot (\omega \wedge \omega')| &\leq |\mathbf{t}'| |\omega \wedge \omega'| = \sin \theta(\omega, \omega') = \{1 - \cos^2 \theta(\omega, \omega')\}^{1/2} \\ &= \{1 - (\omega \cdot \omega')^2\}^{1/2} = \{(1 - \omega \cdot \omega')(1 + \omega \cdot \omega')\}^{1/2} \\ &= \frac{1}{2} |\omega - \omega'| |\omega + \omega'|. \end{aligned}$$

which ensures the boundedness of (3.21). The boundedness of (3.22) follows in a similar way, using (3.23) and the analyticity of $a'_{\nu-\frac{1}{2}}$ on $(-3, 1)$.

To complete the proof consider the case when (3.19) fails, i.e. $\pi - \delta \leq \theta(\omega, \omega') \leq \pi$. For this case recall from (3.5) that $P_{\nu-1/2}(x)$ is analytic for $x \in (-1, 3)$. Therefore (3.1) implies that $L_D(\omega, \omega')$ is bounded for $\pi - \delta \leq \theta(\omega, \omega') \leq \pi$. Thus setting

$$F_D(\omega, \omega) = L_D(\omega, \omega') + \frac{\mathbf{t}' \cdot (\omega \wedge \omega')}{\pi |\omega - \omega'|^2}$$

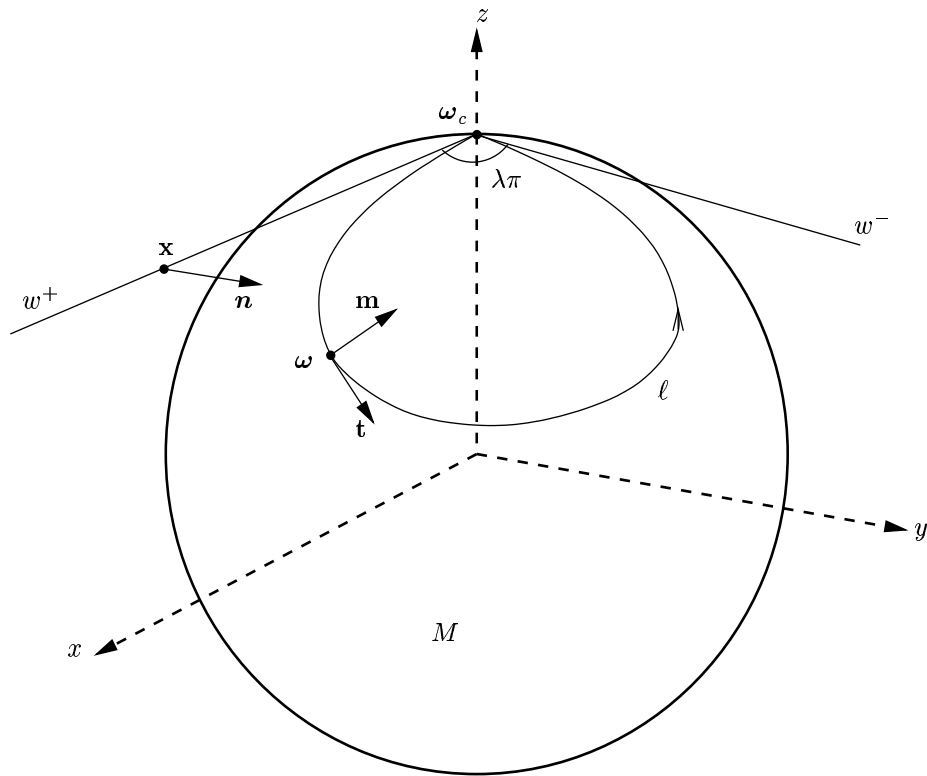


FIG. 3.1. Wedge w and contour ℓ

ensures that (3.10) holds, with $F_D(\omega, \omega')$ bounded for $\pi - \delta \leq \theta(\omega, \omega') \leq \pi$.

(ii) Now suppose that ω is not a corner point and that ω' is sufficiently close to ω so as to ensure that there is no corner point between ω and ω' on ℓ . Let ρ denote an arclength parameterisation of ℓ from any fixed reference point, then setting $\omega = \rho(s)$, the unit tangent \mathbf{t} at ω is given by $\mathbf{t} = \rho_s(s)$, the derivative of $\rho(s)$. Then for ω' near ω with $\omega' = \rho(\sigma)$, we have

$$(3.24) \quad |\omega - \omega'|/|s - \sigma| = O(1) \quad \text{and} \quad |s - \sigma|/|\omega - \omega'| = O(1) \quad \text{as } \sigma \rightarrow s.$$

Also,

$$\omega \wedge \omega' = \rho(s) \wedge \rho(\sigma) = (\rho(s) - \rho(\sigma)) \wedge \rho(\sigma).$$

Hence

$$(3.25) \quad \mathbf{t}' \cdot (\omega \wedge \omega') = \rho_s(\sigma) \cdot ((\rho(s) - \rho(\sigma)) \wedge \rho(\sigma)).$$

Since $|\omega - \omega'|^2 = (\rho(s) - \rho(\sigma)) \cdot (\rho(s) - \rho(\sigma))$, it follows that (3.12) are smooth functions as $\sigma \rightarrow s$ (i.e. $\omega' \rightarrow \omega$). Moreover (3.24) and (3.25) imply that $|\mathbf{t}' \cdot (\omega \wedge \omega')| = O(|\omega - \omega'|^2)$ and so (3.13) follows from (3.21) and (3.22). \square

We see from Theorem 3.3 that if there are no corner points on ℓ , then L_D and L_N are bounded (in fact continuous), so in both the Dirichlet and Neumann cases the integral operator \mathcal{L}_B will be compact on most standard spaces, e.g. $C(\ell), L^2(\ell)$. Then standard stability proofs for the numerical method will follow. However if ℓ does contain a corner, compactness is lost and so another approach is needed to show stability of a numerical method. The approach we will use is to compare the integral operator \mathcal{L}_B with a corresponding plane Laplace integral operator \mathcal{K}_B and then use stability results which are known for the planar Laplace problem. This is done in the following subsection.

3.2. Relation to Planar Laplace Case. To simplify the presentation, we assume that the contour ℓ has one corner which we will denote by the point $\omega_c \in S^2$. The case of several corners is obtained analogously. Without loss of generality, we assume $\omega_c = (0, 0, 1)^T$. Suppose that $\rho(s)$ travels around ℓ with M on the

right-hand side (as indicated by the arrow in Fig. 3.1), as s travels from $-\Lambda$ to Λ , where 2Λ is the length of ℓ . Then we can introduce the “wedge” w in the tangent plane to S^2 at ω_c as follows.

DEFINITION 3.4. *The wedge w is defined to be the union of two straight line segments: $w = w^- \cup w^+$ where*

$$w^- = \{(0, 0, 1)^T + s\mathbf{t}_c^- : s \in [-\Lambda, 0]\}, \quad w^+ = \{(0, 0, 1)^T + s\mathbf{t}_c^+ : s \in [0, \Lambda]\},$$

and $\mathbf{t}_c^\pm = \lim_{s \rightarrow 0^\pm} \boldsymbol{\rho}_s(s)$ (see Fig. 3.1). The angle between the tangents \mathbf{t}_c^+ and $-\mathbf{t}_c^-$ is measured “anti-clockwise” about the z axis (when viewed from outside the sphere) from w^+ to w^- and is denoted $\lambda\pi$, where $\lambda \in (0, 2) \setminus \{1\}$. Without loss of generality we choose our coordinate system so that \mathbf{t}_c^+ is in the direction of the x axis. Each $\mathbf{x} = s\mathbf{t}_c^\pm \in w^\pm$ can be associated with a unique $\boldsymbol{\omega} = \boldsymbol{\rho}(s) \in \ell$, and with a unit normal \mathbf{m} at $\boldsymbol{\omega} \in \ell$ orientated outward from M . To \mathbf{x} we associate a unit normal \mathbf{n} to w in the plane tangent to S^2 at ω_c , orientated so that $\mathbf{n} \cdot \mathbf{m} \rightarrow 1$ as $s \rightarrow 0$. (See also Fig 3.1.) The fundamental solution of Laplace’s equation on the plane is $(1/2\pi) \log |\mathbf{x} - \mathbf{x}'|$. Using this we introduce the operators

$$(\mathcal{K}_B u)(\mathbf{x}) = \int_w K_B(\mathbf{x}, \mathbf{x}') u(\mathbf{x}') d\mathbf{x}', \quad B = D, N.$$

Analogously to (2.12), (2.13), the Dirichlet and Neumann kernels are

$$(3.26) \quad K_D(\mathbf{x}, \mathbf{x}') := \frac{1}{\pi} \frac{\partial}{\partial \mathbf{n}'} \{\log |\mathbf{x} - \mathbf{x}'|\} = -\frac{(\mathbf{x} - \mathbf{x}') \cdot \mathbf{n}'}{\pi |\mathbf{x} - \mathbf{x}'|^2}$$

$$(3.27) \quad K_N(\mathbf{x}, \mathbf{x}') := -\frac{1}{\pi} \frac{\partial}{\partial \mathbf{n}} \{\log |\mathbf{x} - \mathbf{x}'|\} = -\frac{(\mathbf{x} - \mathbf{x}') \cdot \mathbf{n}}{\pi |\mathbf{x} - \mathbf{x}'|^2}.$$

Here \mathbf{n}, \mathbf{n}' are unit normals to ω at $\mathbf{x}, \mathbf{x}' \in w$, as described in Definition 3.4.

Theorem 3.5 will show that the principal singularity of L_B near $\boldsymbol{\omega} = \boldsymbol{\omega}' = \omega_c$ is the same as K_B near $\mathbf{x} = \mathbf{x}' = \omega_c$. This is useful because the properties of the integral operator \mathcal{K}_B with kernel K_B are well-understood [16], [14], [19], [21].

To prepare for Theorem 3.5, we use the arclength parameterisation, $\boldsymbol{\rho}(\sigma)$, of ℓ , introduced above, to rewrite (2.11) on $[-\Lambda, \Lambda]$. Putting $\boldsymbol{\omega} = \boldsymbol{\rho}(s)$ and $\boldsymbol{\omega}' = \boldsymbol{\rho}(\sigma)$ we obtain

$$(3.28) \quad (I + \widehat{\mathcal{L}}_B) \widehat{u} = \widehat{b}_B, \quad \text{with } (\widehat{\mathcal{L}}_B \widehat{u})(s) = \int_{-\Lambda}^{\Lambda} \widehat{L}_B(s, \sigma) \widehat{u}(\sigma) d\sigma, \quad s \in [-\Lambda, \Lambda],$$

where $\widehat{u}(s) = u(\boldsymbol{\rho}(s))$. In the case of Dirichlet boundary data, using (2.12) and Lemma 3.1 we have

$$(3.29) \quad \begin{aligned} \widehat{b}_D(s) &:= -2g_0(\boldsymbol{\rho}(s), \boldsymbol{\omega}_0, \nu) \quad \text{and} \\ \widehat{L}_D(s, \sigma) &:= \frac{1}{2 \cos(\pi\nu)} P'_{\nu - \frac{1}{2}}(-\cos \theta(\boldsymbol{\rho}(s), \boldsymbol{\rho}(\sigma))) \boldsymbol{\rho}_s(\sigma) \cdot (\boldsymbol{\rho}(s) \wedge \boldsymbol{\rho}(\sigma)). \end{aligned}$$

(Note that since $\boldsymbol{\rho}$ is the arclength parameterisation, the Jacobian satisfies $|\boldsymbol{\rho}_s(\sigma)| = 1$ and therefore does not appear explicitly in the kernel.) For Neumann boundary data, using (2.13) and Lemma 3.1 we obtain,

$$(3.30) \quad \begin{aligned} \widehat{b}_N(s) &:= 2 \frac{\partial g_0}{\partial \mathbf{m}(s)}(\boldsymbol{\rho}(s), \boldsymbol{\omega}_0, \nu) \quad \text{and} \\ \widehat{L}_N(s, \sigma) &:= -\frac{1}{2 \cos(\pi\nu)} P'_{\nu - \frac{1}{2}}(-\cos \theta(\boldsymbol{\rho}(s), \boldsymbol{\rho}(\sigma))) \boldsymbol{\rho}_s(s) \cdot (\boldsymbol{\rho}(\sigma) \wedge \boldsymbol{\rho}(s)), \end{aligned}$$

where $\mathbf{m}(s)$ is the corresponding normal to ℓ at $\boldsymbol{\rho}(s)$.

If we now denote the arclength parameterisation of w by \mathbf{r} , with $\mathbf{r}(-\Lambda) = (0, 0, 1)^T - \Lambda \mathbf{t}_c^-$, $\mathbf{r}(0) = \omega_c$ and $\mathbf{r}(\Lambda) = (0, 0, 1)^T + \Lambda \mathbf{t}_c^+$, then we can also rewrite \mathcal{K}_B as an operator

$$(\widehat{\mathcal{K}}_B \widehat{u})(s) = \int_{-\Lambda}^{\Lambda} \widehat{K}_B(s, \sigma) \widehat{u}(\sigma) d\sigma \quad s \in [-\Lambda, \Lambda], \quad B = D, N,$$

where from (3.26), (3.27),

$$(3.31) \quad \widehat{K}_D(s, \sigma) := -\frac{(\mathbf{r}(s) - \mathbf{r}(\sigma)) \cdot \mathbf{n}(\sigma)}{\pi |\mathbf{r}(s) - \mathbf{r}(\sigma)|^2},$$

$$(3.32) \quad \widehat{K}_N(s, \sigma) := -\frac{(\mathbf{r}(s) - \mathbf{r}(\sigma)) \cdot \mathbf{n}(s)}{\pi |\mathbf{r}(s) - \mathbf{r}(\sigma)|^2},$$

for the Dirichlet and Neumann problems respectively. Here $\mathbf{n}(\sigma)$ is the normal to w at $\mathbf{x} = \mathbf{r}(\sigma)$. The following theorem shows that \widehat{K}_B contains the principal singularity of \widehat{L}_B near the corner point $s = \sigma = 0$ in both the Dirichlet and Neumann cases, $B = D, N$.

THEOREM 3.5. *Let $B = D$ or N . Then for $(s, \sigma) \in [-\Lambda, \Lambda] \times [-\Lambda, \Lambda]$, $\widehat{L}_B(s, \sigma) - \widehat{K}_B(s, \sigma)$ is a bounded function.*

Proof. We give the proof for the case $B = D$. The case $B = N$ is analogous. First we consider the kernel \widehat{K}_D . From Definition 3.4 the parametric equation, \mathbf{r} , for w , is given by

$$(3.33) \quad \mathbf{r}(\sigma) = \begin{cases} (-\sigma \cos(\lambda\pi), -\sigma \sin(\lambda\pi), 1)^T, & \sigma \in [-\Lambda, 0] \\ (\sigma, 0, 1)^T, & \sigma \in [0, \Lambda]. \end{cases}$$

Notice that if $-\Lambda \leq s, \sigma \leq 0$ or $0 \leq s, \sigma \leq \Lambda$ then $\mathbf{r}(s)$ and $\mathbf{r}(\sigma)$ lie on the same arm of w and so it follows from (3.31) that $\widehat{K}_D(s, \sigma) = 0$ and, by Theorem 3.3(ii), $\widehat{L}_D(s, \sigma)$ is bounded. So we have to consider only the case when s and σ are on different sides of 0.

First consider the case $-\Lambda \leq s \leq 0 \leq \sigma \leq \Lambda$. Then (3.33) implies that $\mathbf{r}(s) - \mathbf{r}(\sigma) = (-s \cos(\lambda\pi) - \sigma, -s \sin(\lambda\pi), 0)^T$ and $\mathbf{n}(\sigma) = (0, 1, 0)^T$. Therefore $(\mathbf{r}(s) - \mathbf{r}(\sigma)) \cdot \mathbf{n}(\sigma) = -s \sin(\lambda\pi)$ and $|\mathbf{r}(s) - \mathbf{r}(\sigma)|^2 = s^2 + 2s\sigma \cos(\lambda\pi) + \sigma^2$. So from (3.31),

$$(3.34) \quad \widehat{K}_D(s, \sigma) = \frac{1}{\pi} \frac{s \sin(\lambda\pi)}{(s^2 + 2s\sigma \cos(\lambda\pi) + \sigma^2)}, \quad -\Lambda \leq s \leq 0 \leq \sigma \leq \Lambda.$$

A similar calculation shows analogously that

$$(3.35) \quad \widehat{K}_D(s, \sigma) = -\frac{1}{\pi} \frac{s \sin(\lambda\pi)}{(s^2 + 2s\sigma \cos(\lambda\pi) + \sigma^2)}, \quad -\Lambda \leq \sigma \leq 0 \leq s \leq \Lambda.$$

Now we turn our attention to the kernel, $\widehat{L}_D(s, \sigma)$. Using Taylor's theorem we can write the parameterisation $\boldsymbol{\rho}$ as,

$$(3.36) \quad \boldsymbol{\rho}(\sigma) = \begin{cases} \mathbf{r}(\sigma) + \sigma^2(\alpha_1(-\sigma), \beta_1(-\sigma), \gamma_1(-\sigma))^T, & \sigma \in [-\Lambda, 0] \\ \mathbf{r}(\sigma) + \sigma^2(\alpha_2(\sigma), \beta_2(\sigma), \gamma_2(\sigma))^T, & \sigma \in [0, \Lambda], \end{cases}$$

where $\alpha_i(s), \beta_i(s)$ and $\gamma_i(s)$ are smooth functions on $[0, \Lambda]$, for $i = 1, 2$. Thus, for $-\Lambda \leq s \leq 0 \leq \sigma \leq \Lambda$, we have, from (3.36),

$$\boldsymbol{\rho}(s) \wedge \boldsymbol{\rho}(\sigma) = (-s \sin(\lambda\pi), s \cos(\lambda\pi) + \sigma, 0)^T + O(\max\{|s|, |\sigma|\}^2),$$

as $\max\{|s|, |\sigma|\} \rightarrow 0$. Hence with $\boldsymbol{\omega} = \boldsymbol{\rho}(s)$ and $\boldsymbol{\omega}' = \boldsymbol{\rho}(\sigma)$, we have

$$(3.37) \quad \mathbf{t}' = \boldsymbol{\rho}_s(\sigma) = (1, 0, 0)^T + O(|\sigma|),$$

$$-\mathbf{t}' \cdot (\boldsymbol{\omega} \wedge \boldsymbol{\omega}') = s \sin(\lambda\pi) + O(\max\{|s|, |\sigma|\}^2)$$

$$(3.38) \quad \text{and } |\boldsymbol{\omega} - \boldsymbol{\omega}'|^2 = s^2 + 2s\sigma \cos(\lambda\pi) + \sigma^2 + O(\max\{|s|, |\sigma|\}^3),$$

as $\max\{|s|, |\sigma|\} \rightarrow 0$. Therefore we have from (3.10)

$$\widehat{L}_D(s, \sigma) = \frac{\sin(\lambda\pi)}{\pi} \frac{s + \eta_2(s, \sigma)}{s^2 + 2s\sigma \cos(\lambda\pi) + \sigma^2 + \eta_3(s, \sigma)} + \widehat{F}_D(s, \sigma),$$

where $\widehat{F}_D(s, \sigma) = F_D(\boldsymbol{\rho}(s), \boldsymbol{\rho}(\sigma))$ and

$$(3.39) \quad \eta_i(s, \sigma) = O(\max\{|s|, |\sigma|\}^i), \quad i = 2, 3.$$

Hence, for $-\Lambda \leq s \leq 0 \leq \sigma \leq \Lambda$,

$$(3.40) \quad (\widehat{L}_D - \widehat{K}_D)(s, \sigma) = \frac{\sin(\lambda\pi)}{\pi} \left\{ \frac{s + \eta_2(s, \sigma)}{s^2 + 2s\sigma \cos(\lambda\pi) + \sigma^2 + \eta_3(s, \sigma)} - \frac{s}{s^2 + 2s\sigma \cos(\lambda\pi) + \sigma^2} \right\} + \widehat{F}_D(s, \sigma),$$

which is clearly continuous for $(s, \sigma) \neq (0, 0)$.

In order to show that $(\widehat{L}_D - \widehat{K}_D)(s, \sigma)$ is bounded near $(s, \sigma) = (0, 0)$ we need to show that the limit (as $(s, \sigma) \rightarrow (0, 0)$) of the first term on the right-hand side of (3.40) is bounded. We do this for $0 < -s \leq \sigma$. The case $0 < \sigma \leq -s$ is analogous. To obtain the result, write

$$\begin{aligned}
(3.41) \quad & \frac{s + \eta_2(s, \sigma)}{s^2 + 2s\sigma \cos(\lambda\pi) + \sigma^2 + \eta_3(s, \sigma)} - \frac{s}{s^2 + 2s\sigma \sin(\lambda\pi) + \sigma^2} \\
&= \frac{\eta_2(s, \sigma)(s^2 + 2s\sigma \cos(\lambda\pi) + \sigma^2) - \eta_3(s, \sigma)s}{(s^2 + 2s\sigma \cos(\lambda\pi) + \sigma^2)(s^2 + 2s\sigma \cos(\lambda\pi) + \sigma^2 + \eta_3(s, \sigma))} \\
&= \frac{\frac{\eta_2(s, \sigma)}{\sigma^2} \left(\left(\frac{s}{\sigma} \right)^2 + 2 \frac{s}{\sigma} \cos(\lambda\pi) + 1 \right) - \frac{\eta_3(s, \sigma)}{\sigma^3} \frac{s}{\sigma}}{\left(\left(\frac{s}{\sigma} \right)^2 + 2 \frac{s}{\sigma} \cos(\lambda\pi) + 1 \right) \left(\left(\frac{s}{\sigma} \right)^2 + 2 \frac{s}{\sigma} \cos(\lambda\pi) + 1 + \frac{\eta_3(s, \sigma)}{\sigma^2} \right)}.
\end{aligned}$$

Now, when $0 < -s \leq \sigma$ we have $0 < |s| \leq |\sigma|$ and from (3.39) it follows that $\eta_2(s, \sigma)/\sigma^2 = O(1)$, $\eta_3(s, \sigma)/\sigma^3 = O(1)$ and $\eta_3(s, \sigma)/\sigma^2 \rightarrow 0$ as $(s, \sigma) \rightarrow (0, 0)$. Moreover, since $\lambda \in (0, 2) \setminus \{1\}$, we have

$$x^2 + 2x \cos(\lambda\pi) + 1 \geq \sin^2(\lambda\pi) > 0 \quad \text{for all } x \in \mathbb{R}.$$

Combining all these facts with (3.41) shows that the first term in (3.40) is bounded as $(s, \sigma) \rightarrow (0, 0)$. Since \widehat{F}_D is a bounded function it follows that $\widehat{L}_D(s, \sigma) - \widehat{K}_D(s, \sigma)$ is bounded for $-\Lambda \leq s \leq 0 \leq \sigma \leq \Lambda$.

For $-\Lambda \leq \sigma \leq 0 \leq s \leq \Lambda$ the result follows analogously. \square

We shall analyse the equation (3.28) in the space $L^2[-\Lambda, \Lambda]$, equipped with the norm $\|v\|_{L^2[-\Lambda, \Lambda]} = \{\int_{-\Lambda}^{\Lambda} |v(\sigma)|^2 d\sigma\}^{1/2}$. This allows us to cover the Neumann and Dirichlet problems in a unified setting. (There is a corresponding theory in the space $L^\infty[-\Lambda, \Lambda]$ which applies to the Dirichlet problem but not to the Neumann problem.) The next result follows directly from Theorem 3.5, using, e.g. [25, page 326].

COROLLARY 3.6. *For $B = D$ or N , $\widehat{L}_B - \widehat{K}_B$ is a compact operator on $L^2[-\Lambda, \Lambda]$.* \square

The remainder of this section is devoted to proving the well-posedness of (3.28) in $L^2[-\Lambda, \Lambda]$. This is done in Corollary 3.8. Since \widehat{L}_B is a compact perturbation of \widehat{K}_B , the key part of the proof of Corollary 3.8 is contained in the following theorem, which is of key importance also when we come to the numerical analysis in §4.

THEOREM 3.7. *For $B = D$ or N , $(I + \widehat{K}_B)^{-1}$ exists and is bounded on $L^2[-\Lambda, \Lambda]$.*

Proof. Since it follows standard procedures for dealing with Mellin convolution operators we will be brief. More detail is in [13]. The first step is to write the operator $v \mapsto (I + \widehat{K}_B)v$ on $L^2[-\Lambda, \Lambda]$ as two coupled convolution operators on $[0, \Lambda]$. For $(w_1, w_2) \in L^2[0, \Lambda] \times L^2[0, \Lambda]$ we introduce the norm $\|(w_1, w_2)\| = \{\|w_1\|_{L^2[0, \Lambda]}^2 + \|w_2\|_{L^2[0, \Lambda]}^2\}^{1/2}$. Also we define the map $\Pi : L^2[-\Lambda, \Lambda] \rightarrow L^2[0, \Lambda] \times L^2[0, \Lambda]$ by

$$\Pi v := (v_1, v_2), \quad \text{where } v_1(s) = v(-s) + v(s) \quad \text{and} \quad v_2(s) = v(-s) - v(s), \quad s \in [0, \Lambda].$$

Clearly Π is a bijection and $\|\Pi v\|^2 = 2\|v\|_{L^2[-\Lambda, \Lambda]}^2$. Moreover, an elementary calculation using (3.34) and (3.35) and the analogous kernels for $B = N$ (see [13] for details) shows that

$$(3.42) \quad \Pi \widehat{K}_B = \widetilde{\mathbb{K}}_B \Pi, \quad B = D \text{ or } N.$$

Here $\widetilde{\mathbb{K}}_B$ is the matrix operator

$$\widetilde{\mathbb{K}}_B = \begin{pmatrix} \widetilde{\mathcal{K}}_B & 0 \\ 0 & -\widetilde{\mathcal{K}}_B \end{pmatrix},$$

and $\widetilde{\mathcal{K}}_B$ is the Mellin convolution operator on $L^2[0, \Lambda]$ defined by

$$(\widetilde{\mathcal{K}}_B v)(s) = \int_0^\Lambda \widetilde{\kappa}_B(s/\sigma) v(\sigma) \frac{d\sigma}{\sigma},$$

with kernels

$$\widetilde{\kappa}_D(s) = -\frac{\sin(\lambda\pi)}{\pi} \frac{s}{1 - 2s \cos \lambda\pi + s^2}, \quad \widetilde{\kappa}_N(s) = \frac{\sin(\lambda\pi)}{\pi} \frac{1}{1 - 2s \cos \lambda\pi + s^2}.$$

Hence, for all $v \in L^2[-\Lambda, \Lambda]$, we have

$$(3.43) \quad (I + \widehat{\mathcal{K}}_B)v = \Pi^{-1}(I + \widetilde{\mathcal{K}}_B)\Pi v.$$

It can be shown, using Mellin integral transform techniques [19], that $\|\widetilde{\mathcal{K}}_B\|_{L^2[0, \Lambda]} < 1$ (see [13] for further details). Hence by Banach's lemma $I \pm \widetilde{\mathcal{K}}_B$ has a bounded inverse on $L_2[0, \Lambda]$ and the result follows from (3.43). \square

Corollary 3.6 and Theorem 3.7 can now be combined to obtain the well-posedness of (2.11), via the Fredholm alternative. The proof requires the injectiveness of $(I + \widehat{\mathcal{L}}_B)$, i.e. we need to show that for all ν on the contour γ (see Figure 1.2), the implication:

$$(3.44) \quad (I + \widehat{\mathcal{L}}_B)\widehat{u} = 0 \Rightarrow \widehat{u} = 0, \quad \text{for } \widehat{u} \in L^2[-\Lambda, \Lambda].$$

holds.

This implication is established in a standard way using uniqueness results for boundary-value problems for the PDE $\Delta^* + \nu^2 - 1/4$ on the manifolds M and $S^2 \setminus \{M \cup \ell\}$ and the jump relations for the corresponding layer potentials on ℓ . The uniqueness can be easily established because the contour γ is constructed to avoid the eigenvalues of $-\Delta^* + 1/4$ while the jump relations may be found in [18] or [4] for the case of smooth ℓ , and a standard local analysis at corners will provide the extension of the jump relations to corner domains.

COROLLARY 3.8. *For $B = D$ or N , $(I + \widehat{\mathcal{L}}_B)^{-1}$ exists and is bounded on $L^2[-\Lambda, \Lambda]$.*

Proof. Using Theorem 3.7 the left-hand equation in (3.28) can be rewritten as

$$(3.45) \quad (I + (I + \widehat{\mathcal{K}}_B)^{-1}(\widehat{\mathcal{L}}_B - \widehat{\mathcal{K}}_B))\widehat{u} = (I + \widehat{\mathcal{K}}_B)^{-1}\widehat{b}_B.$$

Since, by Corollary 3.6, $(I + \widehat{\mathcal{K}}_B)^{-1}(\widehat{\mathcal{L}}_B - \widehat{\mathcal{K}}_B)$ is a compact operator, it follows from the Fredholm alternative and the injectiveness property (3.44) that (3.45) has a unique solution. It also follows that the operator on the left-hand side of (3.45) has a bounded inverse. Therefore,

$$\|\widehat{u}\|_{L^2[-\Lambda, \Lambda]} \leq C\|(I + \widehat{\mathcal{K}}_B)^{-1}\widehat{b}\|_{L^2[-\Lambda, \Lambda]} \leq C'\|\widehat{b}_B\|_{L^2[-\Lambda, \Lambda]},$$

for some constants C and C' , and the result follows. \square

REMARK 3.9. *If the cone Ξ contains more than one lateral edge, then the contour ℓ will contain several corners. All the results of this subsection remain true in this case. In particular the analogue of Corollary 3.8 ensures the well-posedness of (3.28), or equivalently (2.11) in the multiple corner case. The proof is entirely analogous to the proof above, except that a pair of coupled Mellin convolution equations local to each corner has to be considered. Such systems are standard – see e.g. [14].*

REMARK 3.10. *The operator $\widehat{\mathcal{L}}_B$ depends on the parameter ν and further analysis will be required if one wishes to obtain a “stability bound”, (i.e. a bound on $\|(I - \widehat{\mathcal{L}}_B)^{-1}\|_{L^2[-\Lambda, \Lambda]}$ as a function of ν). However we note that for the case $\nu = i\tau$ the corresponding Helmholtz operator on the plane was analysed in [29], where a stability bound independent of τ was proved. The case $\nu = i\tau$ is particularly important in our computations – see §5.*

4. Numerical Method. In this section we shall discuss the piecewise polynomial collocation method for (3.28) and obtain its convergence, using the results of §3. We also describe briefly its efficient implementation. The performance of this scheme will be illustrated in §5.

The basic collocation scheme is entirely standard, so we will be brief. First introduce a mesh:

$$(4.1) \quad -\Lambda = x_0 < x_1 < \dots < x_m < x_{m+1} < \dots < x_n = \Lambda .$$

We assume here that ℓ has a single corner situated at $x_m = 0$ in parameter space and that $n = 2m$. The case of several corners is similar (see Remark 3.9 and the remarks below (4.5)), and that of a smooth boundary is straightforward (see [13]). We define $I_i = [x_{i-1}, x_i]$ and $h_i = x_i - x_{i-1}$, for $i = 1, \dots, n$. We assume that for each integer $r \geq 1$, we have chosen, *a priori*, r points: $0 < \xi_1^r < \xi_2^r < \dots < \xi_r^r < 1$. Then we introduce the approximation space

$$(4.2) \quad S_n^r[-\Lambda, \Lambda] = \{v \in L^\infty[-\Lambda, \Lambda] : v|_{I_i} \in P_r\} ,$$

where P_r denotes the set of polynomials of order $r \geq 1$ (i.e. of degree $r - 1$). Also, on each I_i , we define the r collocation points $x_{ij}^r = x_{i-1} + h_i \xi_j^r$ and we define the basis functions of $S_n^r[-\Lambda, \Lambda]$ by

$$\phi_{ij}(x) = \begin{cases} \prod_{\substack{1 \leq k \leq r \\ k \neq j}} \frac{x - x_{ik}^r}{x_{ij}^r - x_{ik}^r} \chi_i(x), & \text{when } r > 1 \\ \chi_i(x) & \text{when } r = 1, \end{cases}$$

for $j = 1, \dots, r$ and $i = 1, \dots, n$, where χ_i is the characteristic function on I_i . Clearly $\phi_{ij}|_{I_i} \in P_r$ and $\phi_{ij}(x_{i'j'}) = \delta_{i'i} \delta_{j'j}$.

In the collocation method for (3.28), we seek an approximate solution

$$\hat{u}_n(s) := \sum_{i=1}^n \sum_{j=1}^r \mu_{ij} \phi_{ij}(s),$$

where μ_{ij} are chosen so that the residual vanishes at the collocation points:

$$(4.3) \quad \mu_{i'j'} + \sum_{i=1}^n \sum_{j=1}^r \mu_{ij} \int_{I_i} \hat{\mathcal{L}}_B(x_{i'j'}^r, \sigma) \phi_{ij}(\sigma) d\sigma = \hat{b}_B(x_{i'j'}^r), \text{ for } i' = 1, \dots, n, j' = 1, \dots, r.$$

Equivalently,

$$(4.4) \quad (I + \hat{\mathcal{P}}_n \hat{\mathcal{L}}_B) \hat{u}_n = \hat{\mathcal{P}}_n \hat{b}_B,$$

where $\hat{\mathcal{P}}_n$ denotes the operator onto $S_n^r[-\Lambda, \Lambda]$ defined by interpolation at the points $\{x_{i,j}\}$. Because the ξ_j^r are chosen interior to $[0, 1]$, none of the points x_{ij} are corner points and so $\hat{\mathcal{P}}_n \hat{\mathcal{L}}_B \hat{u}_n$ and $\hat{\mathcal{P}}_n \hat{b}_B$ are well-defined in (4.3).

In the h - version of the collocation method (with r fixed and $n \rightarrow \infty$), we adopt the usual *a priori* mesh grading

$$(4.5) \quad x_{m \pm i} = \pm (i/m)^q \Lambda, \quad \text{for } i = 0, \dots, m,$$

where $q \geq 1$ is the grading exponent. Note that the corner point in parameter space ($x_m = 0$) is a mesh point. This is important. If ℓ has several corners, we would simply use meshes like (4.5) local to each corner, joined together with quasiuniform refinement away from the corners in an obvious way.

To obtain the stability of the collocation scheme, we need the concept of a *modification parameter* $i^* \geq 0$ (first introduced in [14]). The *modified collocation scheme* is exactly the same as (4.3) when $i^* = 0$. But when $i^* \geq 1$, \hat{u}_n is set to 0 on each of the subintervals I_i , $i = m - i^* + 1, \dots, m + i^*$ and (4.3) are required to hold only for $i' \notin \{m - i^* + 1, \dots, m + i^*\}$. (In other words, the collocation solution is set to 0 on each of the $2i^*$ subintervals nearest the corner and (4.3) is not required to hold on those subintervals.) For notational convenience we shall continue to write the collocation equations as (4.4), thus suppressing i^* from the notation.

THEOREM 4.1. *Let r and q be fixed and let $B = D$ or N . Then there exists a modification parameter $i^* \geq 1$ independent of n , and a constant C which may depend on r, q and i^* but not on n such that $\|(I + \hat{\mathcal{P}}_n \hat{\mathcal{L}}_B)^{-1}|_{S_n^r[-\Lambda, \Lambda]} \|_{L^2[-\Lambda, \Lambda]} \leq C$ for all sufficiently large n , i.e. the collocation method (4.4) is stable in $L^2[-\Lambda, \Lambda]$.*

Proof. We shall show that, for each $\epsilon > 0$, there exists a modification such that for n sufficiently large,

$$(4.6) \quad \|(I - \hat{\mathcal{P}}_n) \hat{\mathcal{L}}_B v_n \|_{L^2[-\Lambda, \Lambda]} \leq \epsilon \|v_n \|_{L^2[-\Lambda, \Lambda]},$$

for all $v_n \in S_n^r[-\Lambda, \Lambda]$. Then, since

$$I + \hat{\mathcal{P}}_n \hat{\mathcal{L}}_B = (I + \hat{\mathcal{L}}_B) - (I - \hat{\mathcal{P}}_n) \hat{\mathcal{L}}_B,$$

existence and stability of $(I + \hat{\mathcal{P}}_n \hat{\mathcal{L}}_B)^{-1}$ on $S_n^r[-\Lambda, \Lambda]$ follows from Corollary 3.8.

To obtain (4.6), note that by the triangle inequality,

$$(4.7) \quad \|(I - \hat{\mathcal{P}}_n) \hat{\mathcal{L}}_B v_n \|_{L^2[-\Lambda, \Lambda]} \leq \|(I - \hat{\mathcal{P}}_n) \hat{\mathcal{K}}_B v_n \|_{L^2[-\Lambda, \Lambda]} + \|(I - \hat{\mathcal{P}}_n) (\hat{\mathcal{L}}_B - \hat{\mathcal{K}}_B) v_n \|_{L^2[-\Lambda, \Lambda]}.$$

Now recall that $\widehat{\mathcal{P}}_n$ projects to zero on the $2i^*$ intervals nearest 0. Thus

$$\begin{aligned} \|(I - \widehat{\mathcal{P}}_n)(\widehat{\mathcal{L}}_B - \widehat{\mathcal{K}}_B)v_n\|_{L^2[-\Lambda, \Lambda]}^2 &\leq \|(\widehat{\mathcal{L}}_B - \widehat{\mathcal{K}}_B)v_n\|_{L^2[x_{m-i^*}, x_{m+i^*}]}^2 \\ &\quad + \|(I - \widehat{\mathcal{P}}_n)(\widehat{\mathcal{L}}_B - \widehat{\mathcal{K}}_B)v_n\|_{L^2([-\Lambda, \Lambda] \setminus [x_{m-i^*}, x_{m+i^*}])}^2. \end{aligned} \quad (4.8)$$

By Theorem 3.5, $\widehat{\mathcal{L}}_B - \widehat{\mathcal{K}}_B$ is a bounded function and this implies that $(\widehat{\mathcal{L}}_B - \widehat{\mathcal{K}}_B)$ is compact from $L^2[-\Lambda, \Lambda]$ to $L^\infty[-\Lambda, \Lambda]$, [25, pp. 534-535]. Thus the first term on the right-hand side of (4.8) may be estimated by

$$\begin{aligned} \|(\widehat{\mathcal{L}}_B - \widehat{\mathcal{K}}_B)v_n\|_{L^2[x_{m-i^*}, x_{m+i^*}]}^2 &\leq 2x_{m+i^*} \|(\widehat{\mathcal{L}}_B - \widehat{\mathcal{K}}_B)v_n\|_{L^\infty[x_{m-i^*}, x_{m+i^*}]}^2 \\ &\leq Cn^{-q} \|v_n\|_{L^2[-\Lambda, \Lambda]}^2. \end{aligned} \quad (4.9)$$

(Throughout the proof C denotes a generic constant which is independent of n but may depend on the other parameters.)

We now consider the second term on the right-hand side of (4.8). First we write

$$\begin{aligned} \|(I - \widehat{\mathcal{P}}_n)(\widehat{\mathcal{L}}_B - \widehat{\mathcal{K}}_B)v_n\|_{L^2([-\Lambda, \Lambda] \setminus [x_{m-i^*}, x_{m+i^*}])}^2 &= \sum_{i \leq m-i^*} \|(I - \widehat{\mathcal{P}}_n)(\widehat{\mathcal{L}}_B - \widehat{\mathcal{K}}_B)v_n\|_{L^2(I_i)}^2 \\ &\quad + \sum_{i \geq m+i^*+1} \|(I - \widehat{\mathcal{P}}_n)(\widehat{\mathcal{L}}_B - \widehat{\mathcal{K}}_B)v_n\|_{L^2(I_i)}^2. \end{aligned} \quad (4.10)$$

We will estimate the second sum in (4.10). (The first sum can be dealt with in a similar way.) To do this we recall the standard results for piecewise polynomial interpolation and write

$$\begin{aligned} \sum_{i \geq m+i^*+1} \|(I - \widehat{\mathcal{P}}_n)(\widehat{\mathcal{L}}_B - \widehat{\mathcal{K}}_B)v_n\|_{L^2(I_i)}^2 &\leq C \sum_{i \geq m+i^*+1} h_i^2 \|D(\widehat{\mathcal{L}}_B - \widehat{\mathcal{K}}_B)v_n\|_{L^2(I_i)}^2 \\ &\leq C \sum_{i \geq m+i^*+1} h_i^3 \|s^{-1} sD(\widehat{\mathcal{L}}_B - \widehat{\mathcal{K}}_B)v_n\|_{L^\infty(I_i)}^2. \end{aligned}$$

It can be shown, using the same argument as in the proof of Theorem 3.5, that the operator $sD(\widehat{\mathcal{L}}_B - \widehat{\mathcal{K}}_B)$ has a bounded kernel. Hence, noting that $h_i \leq Cn^{-1}$, we obtain

$$\begin{aligned} \sum_{i \geq m+i^*+1} \|(I - \widehat{\mathcal{P}}_n)(\widehat{\mathcal{L}}_B - \widehat{\mathcal{K}}_B)v_n\|_{L^2(I_i)}^2 &\leq Cn^{-1} \sum_{i \geq m+i^*+1} (h_i x_{i-1}^{-1})^2 \|v_n\|_{L^2[-\Lambda, \Lambda]}^2 \\ &\leq C \max_{i \geq m+i^*+1} (h_i x_{i-1}^{-1})^2 \|v_n\|_{L^2[-\Lambda, \Lambda]}^2. \end{aligned} \quad (4.11)$$

Now for $i \geq i^* + 1$, (4.5) implies

$$h_{m+i} = \left(\frac{i}{m}\right)^q \Lambda - \left(\frac{i-1}{m}\right)^q \Lambda \leq q\Lambda \frac{1}{m} \left(\frac{i}{m}\right)^{q-1}.$$

Hence, since i^* satisfies $i^* \geq 1$,

$$h_{m+i} x_{m+i-1}^{-1} \leq q \frac{1}{m} \left(\frac{i}{m}\right)^{q-1} \left(\frac{m}{i-1}\right)^q \leq Cq \frac{1}{i-1} \leq Cq \frac{1}{i^*}. \quad (4.12)$$

By substituting (4.12) into (4.11) it follows that

$$\sum_{i \geq m+i^*+1} \|(I - \widehat{\mathcal{P}}_n)(\widehat{\mathcal{L}}_B - \widehat{\mathcal{K}}_B)v_n\|_{L^2(I_i)}^2 \leq C \left(\frac{1}{i^*}\right)^2 \|v_n\|_{L^2[-\Lambda, \Lambda]}^2.$$

A similar estimate holds for the first sum in (4.10) and so

$$\begin{aligned} \|(I - \widehat{\mathcal{P}}_n)(\widehat{\mathcal{L}}_B - \widehat{\mathcal{K}}_B)v_n\|_{L^2([-\Lambda, \Lambda] \setminus [x_{m-i^*}, x_{m+i^*}])} &\leq C \frac{1}{i^*} \|v_n\|_{L^2[-\Lambda, \Lambda]} \\ &\leq \frac{\epsilon}{2} \|v_n\|_{L^2[-\Lambda, \Lambda]}, \end{aligned} \quad (4.13)$$

for sufficiently large i^* .

By (4.7), (4.8), (4.9) and (4.13), we see that to prove (4.6) it is sufficient to prove it with $\widehat{\mathcal{L}}_B$ replaced by $\widehat{\mathcal{K}}_B$. However this follows from now-classical results about numerical methods for Mellin convolution equations. To explain briefly, we first employ the operators Π and $\widehat{\mathbb{K}}_B$ defined in the proof of Theorem 3.7, as well as the fact that the mesh (4.1) is symmetric about 0, to obtain $\Pi\widehat{\mathcal{P}}_n\widehat{\mathcal{K}}_B = \widehat{\mathbb{P}}_n\widehat{\mathbb{K}}_B\Pi$ where

$$\widehat{\mathbb{P}}_n = \begin{pmatrix} \tilde{\mathcal{P}}_n & 0 \\ 0 & \tilde{\mathcal{P}}_n \end{pmatrix}.$$

with $\tilde{\mathcal{P}}_n$ defined as the restriction of $\widehat{\mathcal{P}}_n$ to functions on $[0, \Lambda]$. Since $(I - \widehat{\mathcal{P}}_n)\widehat{\mathcal{K}}_B = \Pi^{-1}(I - \widehat{\mathbb{P}}_n)\widehat{\mathbb{K}}_B\Pi$, the result follows if for all $\epsilon > 0$, there exists a modification i^* such that

$$(4.14) \quad \|(I - \tilde{\mathcal{P}}_n)\tilde{\mathcal{K}}_B v_n\|_{L^2[0, \Lambda]} \leq \epsilon \|v_n\|_{L^2[0, \Lambda]},$$

for all $v_n \in S_n^r[0, \Lambda]$ and for sufficiently large n . However result (4.14) follows (even for all n) from the general results in the survey [21]. (See Theorem 3.1 there, and the remarks following it. Note that $\tilde{\kappa}_B$ and $\tilde{\kappa}_N$ both satisfy the conditions (A1) and (A2) of [21], with $p = 2$.) See [22], [14], [19] and also [13] for more details. \square

REMARK 4.2. *The introduction of the parameter i^* is solely a device to prove stability of the collocation method for (2.11) when ℓ contains a corner. No unmodified practical collocation method has ever been observed to be unstable. However the proof that these methods are stable without modification has eluded researchers for 15 years. For this reason and to simplify the presentation we assume that Theorem 4.1 holds for $i^* = 0$ (i.e. no modification) for the remainder of this section. All the following results also hold for $i^* \geq 1$, but the proofs require slightly different technicalities.*

Theorem 4.1 implies that the collocation equation (4.4) is uniquely solvable for all n sufficiently large. An easy manipulation using the equations (3.28) and (4.4) shows that $(I + \widehat{\mathcal{P}}_n\widehat{\mathcal{L}}_B)(\widehat{\mathcal{P}}_n\widehat{u} - \widehat{u}_n) = -\widehat{\mathcal{P}}_n\widehat{\mathcal{L}}_B(I - \widehat{\mathcal{P}}_n)\widehat{u}$. Theorem 4.1 then implies

$$(4.15) \quad \|\widehat{\mathcal{P}}_n\widehat{u} - \widehat{u}_n\|_{L^2[-\Lambda, \Lambda]} \leq C\|\widehat{\mathcal{P}}_n\widehat{\mathcal{L}}_B(I - \widehat{\mathcal{P}}_n)\widehat{u}\|_{L^2[-\Lambda, \Lambda]}.$$

After some technical manipulations using properties of $\widehat{\mathcal{L}}_B = \widehat{\mathcal{K}}_B + (\widehat{\mathcal{L}}_B - \widehat{\mathcal{K}}_B)$ it can be shown that the right-hand side of (4.15) can be bounded by a constant multiple of $\|(I - \widehat{\mathcal{P}}_n)\widehat{u}\|_{L^2[-\Lambda, \Lambda]}$ (see [13]). Then the triangle inequality implies:

$$(4.16) \quad \|\widehat{u} - \widehat{u}_n\|_{L^2[-\Lambda, \Lambda]} \leq \|\widehat{u} - \widehat{\mathcal{P}}_n\widehat{u}\|_{L^2[-\Lambda, \Lambda]} + \|\widehat{\mathcal{P}}_n\widehat{u} - \widehat{u}_n\|_{L^2[-\Lambda, \Lambda]} \leq C\|(I - \widehat{\mathcal{P}}_n)\widehat{u}\|_{L^2[-\Lambda, \Lambda]}.$$

Therefore to obtain convergence rates we need estimates for $\|(I - \widehat{\mathcal{P}}_n)\widehat{u}\|_{L^2[-\Lambda, \Lambda]}$. These of course depend on the regularity of the solution. To describe this regularity we introduce the weighted Sobolev space for an interval $J \subset \mathbb{R}$ and for $k \in \mathbb{N}$ and $\alpha \in \mathbb{R}$:

$$L_{\alpha}^{2,k}(J) = \{v : |x|^{j-\alpha} D^j v \in L^2(J), j = 0, 1, \dots, k\},$$

equipped with the norm $\|v\|_{L_{\alpha}^{2,k}(J)} = \sum_{j=0}^k \|x^{j-\alpha} D^j v\|_{L^2(J)}$, (see [19]).

EXAMPLES 4.3.

(i) *The function*

$$(4.17) \quad \widehat{u}(x) = C' + C''|x|^{\theta}, \quad \text{where } 1/2 < \theta < 1,$$

satisfies $\widehat{u}(x) - C' \in L_{\alpha}^{2,k}[-\Lambda, \Lambda]$ for all $k \geq 0$ and $\alpha < \theta + 1/2$.

(ii) *The function*

$$(4.18) \quad \widehat{u}(x) = C|x|^{\theta-1}, \quad \text{where } 1/2 < \theta < 1,$$

satisfies $\widehat{u}(x) \in L_{\alpha}^{2,k}[-\Lambda, \Lambda]$ for all $k \geq 0$ and $\alpha < \theta - 1/2$.

REMARK 4.4. *When we solve the Dirichlet problem for the Laplace equation in the region interior to a planar polygon using the indirect boundary integral method, the solution of the resulting integral equation has its principal singularity in the form (4.17), where the corner is at $x = 0$ and $\theta = 1/(1 + |\chi|)$, where $(1 - \chi)\pi$ is the angle between the tangents at the corner ($\chi \in (-1, 1) \setminus \{0\}$). When we solve the Neumann problem with*

the same geometry again using the indirect boundary method the density has its principal singularity in the form (4.18), again with $\theta = 1/(1 + |\chi|)$ (see e.g. [16], [22], [19]). It can be shown, by a standard local analysis (see e.g. [31]) that the solutions of our integral equations have the same principal singularity as identified in Examples 4.3. Estimates for $\|(I - \widehat{\mathcal{P}}_n)\widehat{u}\|_{L^2[-\Lambda, \Lambda]}$ under assumptions which encapsulate Examples 4.3(i) and (ii) are well known (see, e.g. [21]). Combining these with (4.16) the final result is given below (see also [13] for more details).

THEOREM 4.5. *Consider the collocation method (4.4) and assume that stability holds in the sense of Theorem 4.1.*

(i) *Suppose that $B = D$ and that the exact solution to (3.28) satisfies $\widehat{u} - C' \in L_\alpha^{2,r}[-\Lambda, \Lambda]$ with $1 < \alpha < 3/2$. Then for sufficiently large n the collocation method described by (4.4) converges with error*

$$(4.19) \quad \|\widehat{u} - \widehat{u}_n\|_{L^2[-\Lambda, \Lambda]} \leq Cn^{-r} \|\widehat{u} - C'\|_{L_\alpha^{2,r}[-\Lambda, \Lambda]} \quad \text{as } n \rightarrow \infty,$$

provided the grading parameter $q \geq \max\{r/\alpha, 1\}$.

(ii) *Suppose that $B = N$ and that the exact solution to (3.28) satisfies $\widehat{u} \in L_\alpha^{2,r}[-\Lambda, \Lambda]$ for some $0 < \alpha < 1/2$. Then for sufficiently large n the collocation method described by (4.4) converges with error*

$$(4.20) \quad \|\widehat{u} - \widehat{u}_n\|_{L^2[-\Lambda, \Lambda]} \leq Cn^{-r} \|\widehat{u}\|_{L_\alpha^{2,r}[-\Lambda, \Lambda]} \quad \text{as } n \rightarrow \infty,$$

provided the grading parameter $q \geq r/\alpha$.

The implementation of the collocation method (4.3) requires the efficient calculation of the stiffness matrix entries

$$(4.21) \quad \widehat{\mathbb{L}}_{i'j',ij} := \int_{I_i} \widehat{L}_B(x_{i'j'}^r, \sigma) \phi_{ij}(\sigma) d\sigma.$$

Each evaluation of the kernel \widehat{L}_B in (4.21) requires an evaluation of (the derivative) of the Legendre function with complex index (see (3.29), (3.30)). We do this by integrating Legendre's differential equation using a Runge-Kutta method – cf. [4, 5, 6, 17] – details are in [13]. Thus efficient quadrature methods for (4.21) are of the utmost importance. This is especially true when we remember that (2.11) needs to be solved many times over (for different values of ν on the imaginary axis) in order to allow the approximate integration of (1.4). The main difficulty in evaluating (4.21) is the singularity which arises when $i' = i$. (This is strongest when I_i contains the origin in parameter space, corresponding to the corner on ℓ .) In [13] a detailed study of quadrature for (4.21) is carried out. Here we have room to mention only the most useful result from [13]:

THEOREM 4.6. *Suppose the collocation points x_{ij}^r , $j = 1, \dots, r$, are chosen to be the r Gauss-Legendre points on $[0, 1]$, shifted to I_i . Suppose that (4.21) is approximated by the Gauss-Legendre rule based at these points for all i, i' satisfying*

$$(4.22) \quad \text{dist}(I_i', I_i) \geq h_i^{1/(r+2)},$$

and the remaining entries of (4.21) are computed exactly. Then the $O(n^{-r})$ convergence rate reported in Theorem 4.5 continues to hold.

Since ϕ_{ij} vanishes at all the points x_{ik}^r , except $k = j$, the implementation of the rule in Theorem 4.6 requires only one kernel evaluation and (4.22) shows that this can be done for most of the matrix as the mesh is refined. It also turns out that even when (4.22) is not satisfied, rules with $O(\log(n))$ kernel evaluations can be employed and the $O(n^{-r})$ rate in Theorem 4.5 remains unperturbed – for more details see §5 and also [13].

5. Numerical Results. We shall illustrate the performance of the numerical method described above in the case of the diffraction of acoustic waves by a *trihedral cone*. In the diffraction literature this is an unsolved *canonical problem* – i.e. it is a relatively simple geometry which often occurs in applications, but there is no known closed form expression for the diffraction coefficients.

Our trihedral cone is determined by three edges which emanate from the origin and pass through the points $\omega_{c_i} \in S^2$, $i = 1, 2, 3$, which are specified by spherical polar coordinates $(\theta^*, 0)$, $(\theta^*, 2\pi/3)$ and $(\theta^*, 4\pi/3)$ respectively, where $\cos \theta^* = 1/\sqrt{3}$. Hence the edges are mutually perpendicular. The conical scatterer Ξ has therefore its surface composed of three mutually perpendicular planar segments determined by each pair of edges and the contour ℓ is made up of three smooth geodesic curves in S^2 , with each pair of smooth curves meeting at an angle of $\pi/2$ at one of the points ω_{c_i} . The geometry is depicted in Fig. 5.1. The contour ℓ is drawn in bold. (This corresponds to the practically important case of the corner of a rectangular building.)

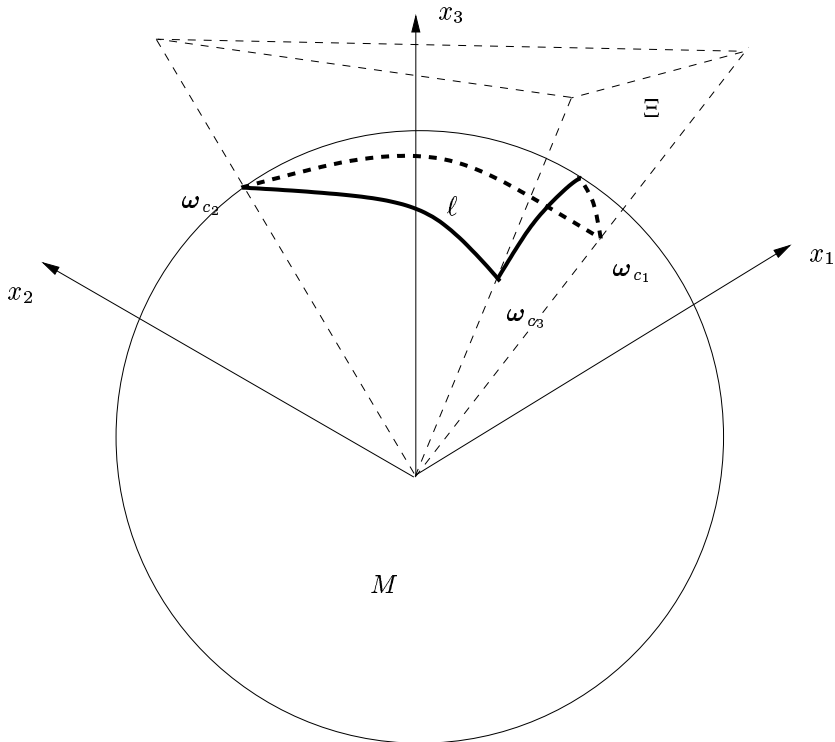


FIG. 5.1. The contour ℓ associated with a trihedral cone

Throughout the computations we used collocation at the Gauss points of subintervals. For the evaluation of the boundary integrals (4.21), we used Gauss quadrature at the collocation points in the “far field”, i.e. when i, i' satisfy (4.22). When (4.22) does not hold we increase the number of quadrature points, d , logarithmically. More precisely, we choose d to be the smallest integer satisfying

$$d \geq \frac{(r+1)\log(n)}{2\log(2)}.$$

This heuristic is motivated by an analysis in [13]. Note that for this geometry, when ω, ω' lie on the same edge of the geodesic triangle ℓ , then $L_B(\omega, \omega') = 0$. Hence one third of the matrix entries are zero. Included in these zero entries are the integrals that occur when the collocation point lies in the interval of integration. Note that our procedure uses only one kernel evaluation for most matrix entries, as mentioned in §4. We shall see that our numerical results coincide with the theoretical predictions of Theorem 4.5.

Our first set of results illustrate the accuracy of methods for solving the integral equation (2.11) (equivalently (3.28)) arising from the boundary value problem (2.5), (2.6). For these tests we set $\omega_0 = -\omega_{c_1}$ and set the parameter $\nu = i$.

The density \hat{u} in (3.28) is not smooth near the corner. In fact, in the case of the Dirichlet problem, we expect from Remark 4.4 that there exists a constant C' such that, $\hat{u} - C' \in L_\alpha^{2,r}$, with $\alpha < 7/6$. (This is because for the corners in this example $\chi = 1/2$, so $\theta = 2/3$ and hence $\theta + 1/2 = 7/6$.) When Neumann boundary conditions are prescribed, we expect $\hat{u} \in L_\alpha^{2,r}$, $\alpha < 1/6$. So, for the Dirichlet problem, piecewise constant approximation ($r = 1$) should (by Theorem 4.5) yield optimal convergence (i.e. $O(n^{-1})$ in the L^2 norm) on a uniform mesh ($q = 1$ in (4.5)). On the other hand for the Neumann problem we expect (by a generalisation of Theorem 4.5) a rate of convergence close to $O(n^{-1/6})$ on a uniform mesh.

To illustrate convergence, for each case we have computed an “exact” solution \hat{u}^* by using piecewise linear collocation on a mesh with 498 nodes. (To obtain the “exact” Dirichlet solution we grade the mesh towards the corners with $q = 2$ and for the the “exact” Neumann solution, since the grading required to obtain optimal convergence is rather severe, we use here a grading exponent $q = 3$.) We computed the approximate L^2 error $\text{err}_n^1 := \|\hat{u}^* - \hat{u}_n\|_2$ using mid-point quadrature with respect to the mesh with n subintervals. The results are given in Table 5.1. As expected, a convergence rate of close to $O(n^{-1})$ is observed for the Dirichlet problem and close to $O(n^{-1/6})$ for the Neumann problem. (In Tables 1-4, “ratio” is defined to be $\text{err}_n^i / \text{err}_{n-1}^i$, for $i = 1$ or 2.) As we have shown, mesh grading will improve suboptimal rates of convergence. Consider the integral

TABLE 5.1

Estimated errors for densities \hat{u} using the piecewise constant collocation method for (3.28) on a uniform mesh $q = 1$

n	Dirichlet Problem		Neumann Problem	
	err_n^1	ratio	err_n^1	ratio
24	9.957E-2		1.609E-3	
48	5.285E-2	1.88	1.530E-3	1.05
96	2.472E-2	2.14	1.229E-3	1.24
192	1.074E-2	2.30	1.077E-3	1.14
384	4.992E-3	2.15	9.589E-4	1.12

equation arising from the Neumann problem. Because its solution satisfies $\hat{u} \in L_\alpha^{2,r}$, with $\alpha < 1/6$, it can be shown (by the methods of Theorem 4.5) that with $q' \leq 6r$ a rate of convergence of $O(n^{-q'/6})$ in the L^2 norm can be attained when a graded mesh is used with grading exponent $q > q'$ for collocation onto piecewise polynomials of order r . We illustrate the correctness of this result with $q = 3$. The results are in Table 5.2. Here we find that the Neumann problem now converges with rate close to $O(n^{-1/2})$, as expected. The

TABLE 5.2

Estimated errors for densities \hat{u} , using the piecewise constant collocation method for (3.28) on a graded mesh, $q=3$

n	Dirichlet Problem		Neumann Problem	
	err_n^1	ratio	err_n^1	ratio
24	1.257E-2		6.307E-3	
48	4.948E-3	2.54	6.106E-3	1.03
96	2.147E-3	2.30	4.744E-3	1.29
192	7.842E-4	2.74	3.553E-3	1.34
384	2.442E-4	3.21	2.738E-3	1.30

Dirichlet problem now appears to converge with a superoptimal rate, but this could be expected to subside back to $O(n^{-1})$ asymptotically. These results indicate that our integral equation solver is working as predicted by the theory.

Our next set of results illustrate the convergence of the approximate solutions to the spherical boundary-value problem (2.5), (2.6). We consider the same problem as above with $\omega_0 = -\omega_{c_1}$, and $\nu = i$. In Tables 5.3 and 5.4, we tabulate the errors in approximate solutions to (2.5), (2.6) obtained by substituting $u_n(\rho(s), \nu) = \hat{u}_n(s)$ into (2.7) (in the Dirichlet case) and (2.9) (in the Neumann case) and computing the resulting integrals by the Gauss quadrature rule based at the points used in the computation of \hat{u}_n . For illustration we have chosen to observe the solution at the particular observation direction $\omega = (0, 0, -1)$. The error err_n^2 is computed by $|g_n^r(\omega, \omega_0, \nu) - \tilde{g}^r(\omega, \omega_0, \nu)|$ where \tilde{g}^r is computed with a large n ($= 330$) and $q = 3$.

The results illustrate the superconvergence of the method (well-documented in the case of planar problems (e.g. [14, 3, 21]), with close to $O(n^{-2})$ convergence attained for $q = 3$. The extreme gradings needed for optimal convergence of the density may not be needed for the potential, and in fact better than optimal convergence may be obtained because of the smoothness of the fundamental solution away from the boundary ℓ .

We emphasise that the results in Tables 5.1 - 5.4 illustrate not only the convergence theory in §4, but also show that the algorithm used to compute the Legendre functions with complex index (by applying a Runge-Kutta method to Legendre's differential equation), which is described in detail in [13], is working in a stable manner.

TABLE 5.3

Estimated errors for the potential (2.7) using the piecewise constant collocation method (Dirichlet boundary conditions)

n	Uniform mesh, q=1		Graded mesh, q=2		Graded Mesh, q=3	
	err_n^2	ratio	err_n^2	ratio	err_n^2	ratio
12	3.12E-4		3.16E-4		4.70E-4	
24	1.36E-4	2.3	1.35E-4	2.4	1.62E-4	2.9
48	5.43E-5	2.5	4.21E-5	3.2	6.12E-5	2.7
96	2.13E-5	2.6	1.34E-5	3.2	2.02E-5	3.0
192	8.84E-6	2.4	4.09E-6	3.3	5.91E-6	3.4

TABLE 5.4

Estimated errors for the potential (2.9) using the piecewise constant collocation method (Neumann boundary conditions)

	Uniform mesh, q=1		Graded mesh, q=2		Graded Mesh, q=3	
n	err _n ²	ratio	err _n ²	ratio	err _n ²	ratio
12	6.25E-5		3.74E-5		4.45E-5	
24	2.68E-5	2.3	1.02E-5	3.7	8.07E-6	5.5
48	1.11E-5	2.4	2.93E-6	3.5	3.08E-6	2.6
96	4.54E-6	2.5	7.72E-7	3.8	8.73E-7	3.5
192	1.82E-6	2.5	2.05E-7	3.8	2.35E-7	3.7

The results given here involve approximation with piecewise constant basis functions. Results for piecewise linears are given in [13]. An important point is that, since only one kernel evaluation is needed for most matrix entries *independent* of the order of the basis functions, the cost of implementation does not increase much as the order of the basis functions is increased. This suggests that the $h - p$ version of the boundary element method should be very competitive for this application and our next set of results concern this method.

For fixed $\sigma \in (0, 1)$ we define a geometrically graded mesh on $[-\Lambda, \Lambda]$ by

$$(5.1) \quad x_{m+i} = \sigma^{m-i}\Lambda, \quad -x_{m-i} = \sigma^{m-i}\Lambda \quad i = 1, \dots, m \quad x_m = 0.$$

Instead of seeking an approximate solution in the space S_n^r of piecewise polynomials of fixed order r on each subinterval, we allow a variable order r_i on each subinterval I_i (see (4.1) and the remarks following). A typical distribution of orders would be :

$$r = \lceil (m+1-i)\beta \rceil \text{ for } i < m, \quad r = \lceil (i-m)\beta \rceil \text{ for } i > m+1$$

for some fixed parameter $\beta > 0$, where, for $x \in \mathbb{R}$, $\lceil x \rceil$ denotes the smallest integer which is strictly greater than x . On the intervals I_i , $i = m, m+1$ the approximate solution is set to zero. Thus, on intervals close to the corner we approximate the solution on small subintervals, using low order methods, while further away we use higher orders on larger subintervals. The maximum order increases linearly with m and hence also with n . This is a standard prescription (e.g. [20]).

By making use of the fundamental results of Elschner ([20]) for the Laplace case, and combining these with our results in §3, it can be shown [13] that the $h - p$ method is stable. By making further assumptions about the regularity of the solution to (3.28), it can be shown that the $h - p$ method converges exponentially. In Fig. 5.2 we illustrate the convergence of the $h - p$ method, compared with the piecewise constant and piecewise linear cases for the potentials (2.7) arising from the Dirichlet problem with $\omega_0 = -\omega_{c_1}$, $\omega = (0, 0, -1)$ and $\nu = i$.

In these computations, the parameter values $\sigma = 0.25$ and $\beta = 0.5$ were employed in the $h - p$ method. For these results we naively used the r -point Gauss-Legendre rule to calculate the matrix entries $\mathbb{L}_{i',j',ij}$, i.e. in this case *all* of the matrix entries were computed using one kernel evaluation. Observe the exponential convergence of the $h - p$ method in Fig. 5.2. (For another way to obtain exponential convergence for this type of integral equation, see [28].)

Finally, in order to illustrate the computations of the diffraction coefficients for this geometry, we shall show graphically how the computed $f(\omega, \omega_0)$ in (1.4) varies for three different incidence directions ω_0 , and many observation directions ω ranging over a subdomain of M . In this illustration we restrict to the Dirichlet problem, we consider the incident directions given in spherical polar coordinates (θ, ϕ) by

$$(5.2) \quad \omega_0 = (\pi, 0), \quad (11\pi/12, 0), \quad \text{and} \quad (5\pi/6, 0),$$

and a range of observation directions

$$(5.3) \quad \omega = ((\pi - \theta), \phi), \quad \text{with} \quad 0 \leq \theta \leq \pi/3, \quad 0 \leq \phi \leq 2\pi.$$

In Fig. 5.3 we illustrate how $|f(\omega, \omega_0)|$ varies as a function of θ and ϕ , for each of the three different incident angles. The quantity $|f(\omega, \omega_0)|$ is plotted on the x_3 axis against the projection of ω onto the x_1x_2 -plane given by: $\omega = (\pi - \theta, \phi) \mapsto (\theta \cos \phi, \theta \sin \phi)$.

Observe in the first row of Fig. 5.3 that when $\omega_0 = (\pi, 0)$, i.e. the incident wave propagates in an ‘‘axial’’ direction, then the magnitude of the diffraction coefficients is smallest in the backscattering direction. This is

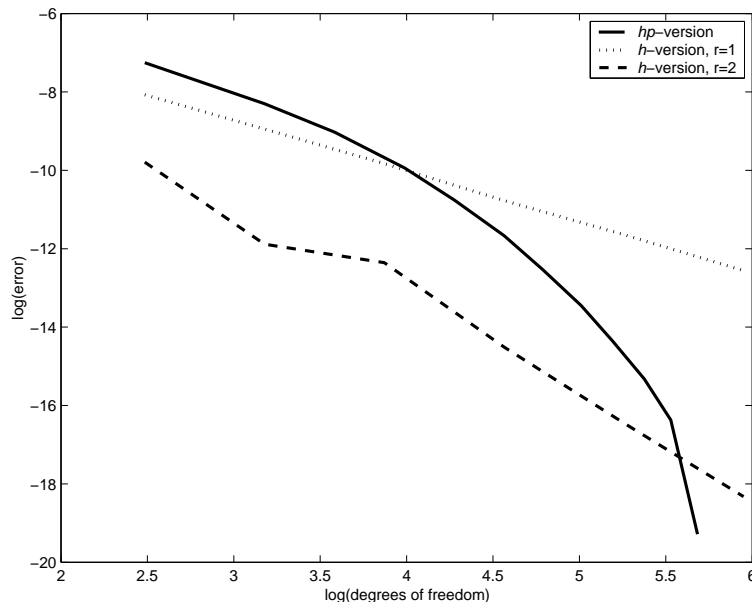


FIG. 5.2. Errors for the potential (2.7) for the h -version and h - p -version of collocation

in qualitative agreement with results for the circular cone [4]. Also note when $\omega_0 = (\pi, 0)$ that if we fix $\theta > 0$ then the distance between $\omega = (\pi - \theta, \phi)$ and the boundary of the nonsingular region, given by $\theta_1(\omega, \omega_0) = \pi$ – see (2.1), is smallest when $\phi = 0, 2\pi/3, 4\pi/3$. At the singular directions f is infinitely large hence the three peaks appear in the first row of Fig. 5.3.

As expected, the results are symmetric with respect to rotations by $\pm 2\pi/3$ about the axis. As we vary the angle of incidence, the symmetry breaks and the position of the singular directions will vary. In particular it can be shown from (2.1) that for $\omega_0 = (11\pi/12, 0)$ and $(5\pi/6, 0)$, and fixed $\theta > 0$ the distance between ω and the singular directions is smallest when $\phi = 0$. This explains the faster growth, as θ increases, of $|f(\omega, \omega_0)|$ along $\phi = 0$ (i.e. along the line $x_2 = 0$) – see the second and third rows of Fig. 5.3.

The numerical method used for these computations was the piecewise constant collocation method with $n = 48$ subintervals on a uniform mesh (cf. Theorem 4.5). To produce each picture in Fig. 5.3 the density in the integral equation (3.28) was approximated for 80 values of ν . Then using these densities we computed the solution to the BVP (2.5), (2.6) for the same 80 values of ν at ~ 800 observation points ω . Therefore $\sim 64,000$ evaluations of the double layer potential were required. The diffraction coefficient f was computed from formula (1.4) by truncation to a finite domain of integration with respect to $\nu = i\tau$ and then applying the trapezoidal rule. The truncation points are chosen according to an analysis of the asymptotics of the integrand in (1.4) for large $|\tau|$ and are designed to yield an overall method which converges at the same rate as the method for computing g^r (see [13]). Clearly this is a very computationally intensive problem and the efficiency of our algorithm is of prime importance.

Acknowledgement We thank Simon Chandler-Wilde for his helpful comments on this work.

REFERENCES

- [1] M. Abramowitz and I.A. Stegun. *Handbook of Mathematical Functions*. Dover Publications, New York, 1965.
- [2] Y.A. Antipov, Diffraction of a plane wave by a circular cone with an impedance boundary condition, *SIAM J. Appl. Math.*, 62:1122–1152, 2002.
- [3] K.E. Atkinson. *The Numerical Solution of Integral Equations of the Second Kind*. Cambridge University Press, Cambridge, 1997.
- [4] V.M. Babich, D.B. Dement'ev, and B.A. Samokish. On the diffraction of high-frequency waves by a cone of arbitrary shape. *Wave Motion*, 21:203–207, 1995.
- [5] V.M. Babich, V.P. Smyshlyaev, D.B. Dement'ev, and B.A. Samokish. Numerical calculation of the diffraction coefficients for an arbitrarily shaped perfectly conducting cone. *IEEE Trans. Antennas & Propagation*, 44:740–747, 1996.
- [6] V.M. Babich, D.B. Dement'ev, B.A. Samokish, and V.P. Smyshlyaev. On evaluation of the diffraction coefficients for arbitrary "nonsingular" directions of a smooth convex cone. *SIAM J. Appl. Math.*, 60:536–573, 2000.
- [7] V.M. Babič and V.S. Buldryev. *Short-Wave-Length Diffraction Theory*. Springer-Verlag, Berlin, 1991.

- [8] V.M. Babich and V.V. Kamotski, Computation of the scattering amplitude of a wave diffracted by the vertex of a cone of arbitrary shape, *Journal of Mathematical Sciences*, 108(5):635–641, 2002.
- [9] J.M.L. Bernard Méthode analytique et transformées fonctionnelles pour la diffraction d'ondes par une singularité conique, Rapport CEA-R-5764 Editions Dist/Saslay, 1997.
- [10] J.M.L. Bernard and M.A. Lyalinov, Electromagnetic scattering by an impedance cone, to appear in *Quarterly J. of Mechanics and Applied Mathematics*, 2004.
- [11] V.A. Borovikov, *Diffraction by Polygons and Polyhedrons*, Nauka, Moscow, 1966.
- [12] J.J. Bowman, T.B.A. Senior, and P.L.E. Uslenghi. *Electromagnetic and Acoustic Scattering by Simple Shapes*. North-Holland, Amsterdam, 1969. Revised 1987.
- [13] B.D. Bonner. *Calculating Conical Diffraction Coefficients*. PhD thesis, University of Bath, 2003. http://www.maths.bath.ac.uk/~igg/Bonner_Thesis.pdf
- [14] G.A. Chandler and I.G. Graham. Product integration-collocation methods for noncompact integral operator equations. *Math. Comp.*, 50:125–138, 1988.
- [15] J. Cheeger and I.M. Taylor, On the diffraction of waves by conical singularities I and II, *Comm. Pure Appl. Math.* 35:275-331, 487-529, 1982.
- [16] M. Costabel and E.P. Stephan. Boundary integral equations for mixed boundary value problems in polygonal domains and Galerkin approximation. In *Mathematical Models and Methods in Mechanics*, volume 15, pages 175–251. Banach Centre Publications, PWN, Warsaw, 1985.
- [17] D.B. Dement'ev, B.A. Samokish and V.M. Babich, Computation of the Legendre function, Unpublished manuscript, 2000.
- [18] R. Duduchava. Boundary value problems on a smooth surface with smooth boundary. *Universität Stuttgart, Preprint 2002-5*, 1–19, 2002.
- [19] J. Elschner. On spline collocation for convolution equations. *Integral Equations and Oper. Theory*, 12:486–510, 1989.
- [20] J. Elschner. The h-p-version of spline approximation methods for Mellin convolution equations. *J. Integral Equations and Appl.*, 5(1):47–73, 1993.
- [21] J. Elschner and I.G. Graham. Numerical methods for integral equations of Mellin type. *J. Comp. Appl. Math.*, 125:423–437, 2000.
- [22] I.G. Graham and G.A. Chandler. High-order methods for linear functionals of solutions of second kind integral equations. *SIAM J. Numer. Anal.*, 25:1118–1137, 1988.
- [23] E.W. Hobson. *The Theory of Spherical and Ellipsoidal Harmonics*. Cambridge University Press, Cambridge, 1931.
- [24] V.V. Kamotski, Calculation of some integrals describing wave fields, *Journal of Mathematical Sciences*, 108(5):665–673, 2002.
- [25] L.V. Kantorovich and G.P. Akilov. *Functional Analysis*. Pergamon, Oxford, 1982.
- [26] J.B. Keller. Diffraction by a convex cylinder. *IRE Trans. Ant. Prop.*, 4:312–321, 1956.
- [27] J.B. Keller. The geometrical theory of diffraction. *J. Opt. Soc. Amer.*, 52:116–130, 1962.
- [28] R. Kress. A Nyström method for boundary integral equations in domains with corners *Numer. Math.*, 58: 145–161, 1990.
- [29] S. Langdon and I.G. Graham. Boundary integral methods for singularly perturbed boundary value problems, *IMA J. Numer. Anal.* 21: 217-237, 2001.
- [30] W. McLean. *Strongly Elliptic Systems and Boundary Integral Equations*, Cambridge University Press, Cambridge, 2000.
- [31] H. Schmitz, K. Volk and W.L. Wendland. Three-dimensional singularities of elastic fields near vertices. *Numerical Methods for Partial Differential Equations*, 9: 323–337, 1993.
- [32] V.P. Smyshlyaev. Diffraction by conical surfaces at high frequencies. *Wave Motion*, 12:329–339, 1990.
- [33] V.P. Smyshlyaev. The high-frequency diffraction of electromagnetic waves by cones of arbitrary cross-sections. *SIAM J. Appl. Math.*, 53:670–688, 1993.

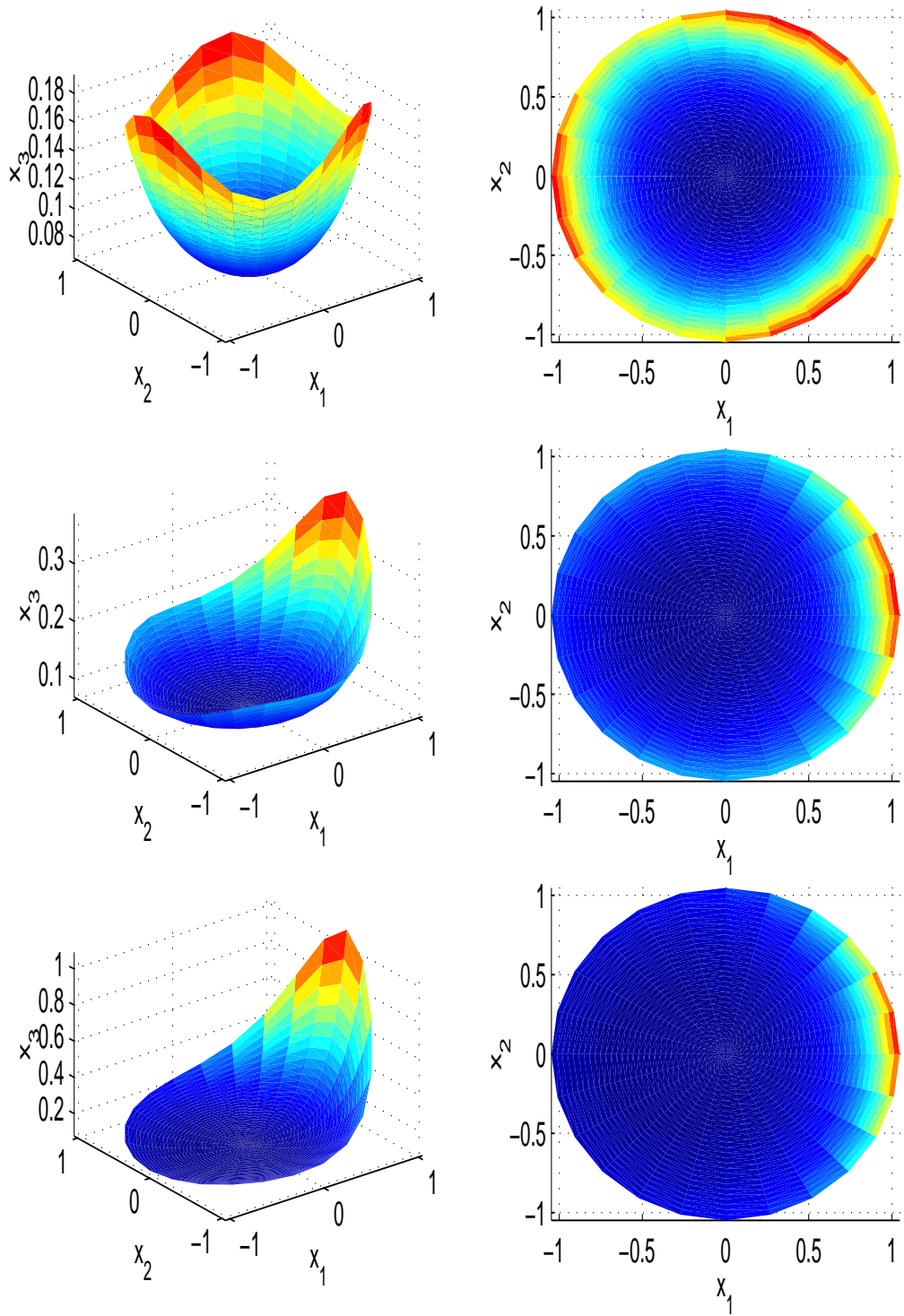


FIG. 5.3. Diffraction coefficients for a trihedral cone.